Future Circular Collider

PUBLICATION

Preliminary collimation system design concept and performance estimate: Deliverable D2.6

Bruce, Roderik (CERN) *et al.*

01 March 2019

The research leading to this document is part of the Future Circular Collider Study

The electronic version of this FCC Publication is available on the CERN Document Server at the following URL :
<http://cds.cern.ch/record/2665192>

PRELIMINARY COLLIMATION
SYSTEM DESIGN CONCEPT AND
PERFORMANCE ESTIMATE

EuroCirCol-P3-WP2-
D2.6, EDMS
2041777

Date: 27/02/2019

Grant Agreement No. 654305

EuroCirCol

European Circular Energy-Frontier Collider Study

Horizon 2020 Research and Innovation Framework Programme, Research and Innovation Action

DELIVERABLE REPORT

PRELIMINARY COLLIMATION SYSTEM DESIGN CONCEPT AND PERFORMANCE ESTIMATE

Document identifier:	EuroCirCol-P3-WP2-D2.6, EDMS 2041777
Due date:	End of month 45 (March 1, 2019)
Report release date:	27/02/2019
Work package:	WP2 (Arc lattice design))
Lead beneficiary:	CEA
Document status:	RELEASED (V1.0)

Abstract:

Description of the collimation system baseline design including a list of beam-line elements (type, description, quantity, physical element characteristics). Description of the assumptions, requirements and constraints on the infrastructure and services. Summary of the expected performance.

Delivery Slip

	Name	**Partner**	**Date**
Authored by	Roderik Bruce James Molson	CERN	27/02/19
Edited by	Julie Hadre Johannes Gutleber	CERN	01/03/19
Reviewed by	Michael Benedikt Daniel Schulte	CERN	28/02/19
Approved by	EuroCirCol Coordination Committee		01/03/19

TABLE OF CONTENTS

**PRELIMINARY COLLIMATION
SYSTEM DESIGN CONCEPT AND
PERFORMANCE ESTIMATE**

*EuroCirCol-P3-WP2-
D2.6, EDMS
2041777*

Date: 27/02/2019

1 INTRODUCTION

In order to achieve a high luminosity at 50 TeV, a high beam current is required in the FCC-hh. Combined with the 50 TeV particle energy, this results in a stored beam energy of about 8.3 GJ, assuming the baseline parameters of 10400 bunches of 10^{11} protons per bunch. This is about a factor 24 higher than the nominal LHC and a factor 12 higher than the HL-LHC. Therefore, the FCC-hh beams are highly destructive and open up a new regime in terms of machine protection considerations. Absorbing the energy of even very small beam losses becomes challenging.

To achieve the high per particle energy, strong magnetic fields are needed, which demands the usage of superconducting magnets operating at cryogenic temperatures. A loss of a small fraction of the beam can deposit enough energy such that the induced heat in a cold magnet moves it to a normal-conducting state, known as a quench. To avoid this, a collimation system must be installed to protect the magnets from beam losses, which is the main topic of this chapter. The development of the design of the various aspects of FCC-hh collimation has been documented in previous publications [1, 2, 3, 4].

In addition to the regular cleaning losses that are expected to occur routinely, the collimation system must also protect machine elements against damage during irregular and accidental beam losses that could occur, e.g. injection and extraction kicker miss-fires, or failures of other elements. If needed, the collimators can be sacrificed in order to prevent beam losses into more critical locations, such as the experimental detectors. Furthermore, the collimation system should also localise the losses and hence the radiation dose to controlled areas, and if needed help in reducing machine-induced experimental backgrounds, all while keeping the machine impedance within acceptable limits.

Beam loss rates in the FCC-hh are very hard to predict and depend on a number of unknowns, but regular operation and tuning of the machine requires that a reasonable range of beam lifetimes (BLT) can be handled without a beam dump, quench or collimator damage. For the design and specification of the collimation system, we assume as a target that the FCC-hh should be able to sustain betatron losses due to a BLT drop down to 12 minutes over a time period of 10 s, and a BLT of 1 h in steady state. The former scenario corresponds to an extreme instantaneous beam loss power of 11.6 MW. These design scenarios have been taken over from the LHC design [5]. Although LHC operation in Run 2 has very rarely resulted in such pessimistic losses, these criteria are conservatively taken over for the FCC-hh design.

For off-momentum losses, the most critical scenario is taken to be the losses at the start of the energy ramp, where any off-energy tail outside of the RF buckets is rapidly lost as the acceleration starts [6]. Based on LHC experience, we use as a design criterion for the collimation system that the machine should be able to routinely handle losses of 1% of the total beam intensity over 10 s [7]. This assumes that the rate of change of the energy at the start of the ramp is similar to that of the LHC.

The baseline FCC-hh collimation system is based on the experience of the design and operation of the LHC system [8, 9, 10, 11, 12, 13, 14], as well as foreseen upgrades for HL-LHC [15, 16, 17, 18, 19].

The baseline concept and layout of the collimation insertions for FCC-hh are described in Sec. 2, and the geometric considerations for protecting the machine aperture are shown in Sec. 3. The cleaning performance of the system is assessed in Sec. 4 through tracking simulations, which are used to estimate the resulting beam loss pattern and power loads around the ring for various

expected loss scenarios. Detailed energy deposition studies are presented for the most critical cold region in Sec. 5 and for the warm betatron cleaning insertion in Sec. 6. The thermo-mechanical response of the most loaded collimators during expected loss scenarios is investigated in Sec. 7, while an outlook on future developments is given in Sec. 8.

2   BASELINE COLLIMATION CONCEPT AND LAYOUT

Two main collimation insertions are used; a betatron system in IRJ for removing particles that have a large amplitude in transverse phase space, and a momentum collimation system in IRF, for removing particles with a large rigidity offset. In addition to these two insertions, collimators exist around each experimental insertion, for both the incoming and outgoing beams. Finally collimators are placed around the injection and extraction regions to protect against failure cases.

In IRJ and IRF, a multi-stage cleaning system is used, which is a scaled-up version of the LHC system. It has primary collimators (TCP) closest to the beam, followed by secondary collimators (TCS), and absorbers (TCLA). As for the LHC, the main bottleneck in terms of cleaning losses is expected for the FCC-hh to be in the dispersion suppressor (DS) downstream of the betatron collimation insertion, where the dispersion generated due to the superconducting dipoles increases rapidly. Protons that have lost energy in single diffractive scattering in the TCP and have a small enough angular deviation to bypass the TCSs risk to be lost there [12]. In order to alleviate these losses, it is planned to install DS collimators (TCLD) in the cold region, similarly to the upgrades planned for HL-LHC [15]. It is planned to install TCLDs in IRF as well, and also downstream of the experiments in order to catch off-energy collsion debris that otherwise risk to put a too high load on the DS. The optics and collimator positions in IRJ and IRF are shown in Figures 1–4, and the full list of collimators with their names, positions, materials, settings through the cycle, and orientations are shown in Table 1.

The baseline betatron collimation insertion is a scaling of the current LHC system, under the constraint that there is a minimum mechanically feasible jaw gap size. In order to keep similar settings as the LHC in units of beam σ, the smaller geometric emittance of the 50 TeV beam is compensated by a larger β-function.
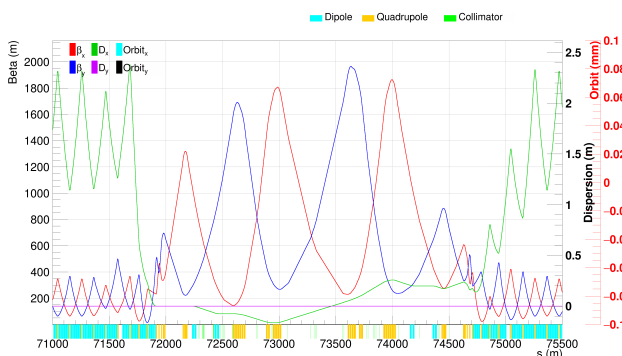

Figure 1: The optics in the betatron collimation insertion - (IRJ) at injection configuration.
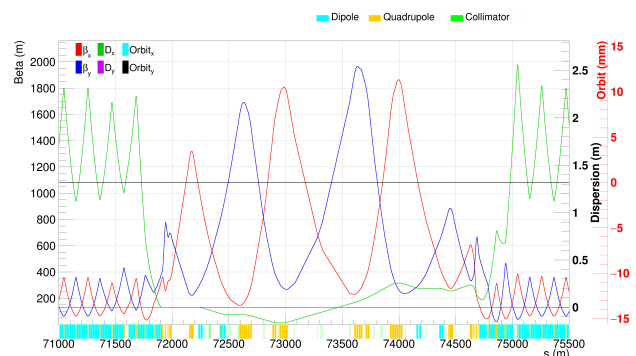

Figure 2: The optics in the betatron collimation insertion (IRJ) at collision configuration.
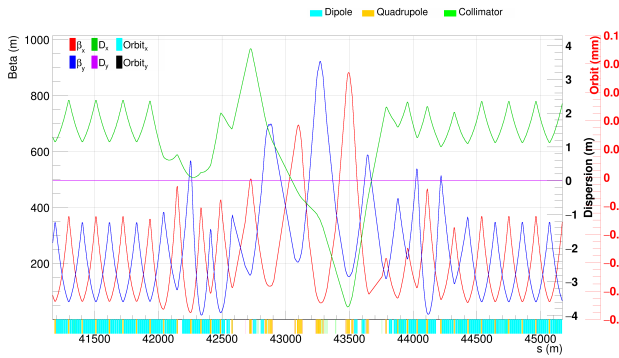
Figure 3: The optics in the energy collimation insertion - IRF at injection configuration.
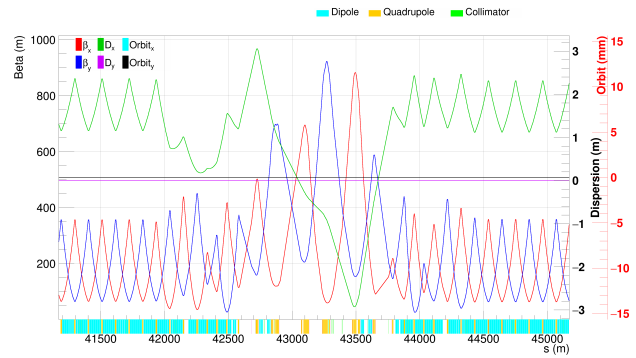

Figure 4: The optics in the energy collimation insertion (IRF) at collision configuration.

Therefore, all β-functions have been scaled by $\sqrt{\frac{E_{FCC}}{E_{LHC}}} = \sqrt{\frac{50}{7}} \approx 2.67$. To achieve this, all magnet lengths and separations have been increased by 2.67, and the total length of the insertion is 2.7 km. This ensures that the magnetic fields in the warm magnets are of the same magnitude and therefore can be constructed. The increase in focusing required from the energy increase over the LHC comes from the increase in magnetic length.

For the momentum cleaning insertion, the baseline is also a layout similar to the LHC but scaled up by the same factor as the betatron system. This is the lattice used for the studies presented later in this report. However, work on alternative designs is underway, and a first version of a new optics for the off-momentum cleaning insertion has been conceived. This is based on an optimization of the normalized dispersion at the off-momentum TCP, while keeping favourable phase advances to secondary and tertiary collimators. This alternative design has shown some first promising results in terms of geometric acceptance and protection of the downstream arc, however, more work is needed on the optimization of potential aperture bottlenecks at injection, as well as tracking studies to optimize the collimator placement.

The collimators for the present studies are assumed to be of a design similar to those used in the LHC, i.e. pairs of movable collimator jaws constructed of sections of amorphous materials, with a single tank per beam for each collimator. The requirements on infrastructure are also similar. Cooling water is required, and the controls infrastructure needs to be adequately implemented and no sensitive electronic components can be placed in areas where they risk radiation damage. A previous design of the FCC-hh lattice, with the extraction kickers placed close to the collimators, was abandoned due to the high radiation load to the kickers. Since the collimation insertion will be a high-radiation area, remote inspection and handling capabilities would be highly beneficial in order to reduce the dose to personnel.

The TCPs and TCSs need to be rather robust. It is foreseen to use carbon-fibre composite (CFC) for the TCPs and the first TCS, which are the most critical devices in terms of robustness, while molybdenum-graphite (MoGr) with a 5 μm coating of Mo is used for the downstream TCSs, which are less loaded. This allows the machine impedance to be reduced to acceptable levels. This material, which is foreseen to be used in the HL-LHC [15], has a significantly lower impedance than CFC. In this report it is assumed that such collimators can be reliably produced within specifications. Using coated graphite has been considered as a backup solution. Iterations

**PRELIMINARY COLLIMATION
SYSTEM DESIGN CONCEPT AND
PERFORMANCE ESTIMATE**

**EuroCirCol-P3-WP2-
D2.6, EDMS
2041777**

Date: 27/02/2019

on the mechanical design, with improvements on the LHC solution, could be done in the future to ensure optimum response from the whole collimator structure to the expected loads.

Other collimators, such as the TCLAs and the tertiary collimators (TCTs) in the experimental insertions, are further away from the beam center and have lower requirements on robustness but higher requirements on absorption. As in the LHC, these collimators are made of a heavy tungsten alloy (Inermet 180).

Collimator	Material	Number	Injection ($n\sigma$)	Collision ($n\sigma$)
β TCP	CFC	2	7.6	7.6
β TCSG	CFC/MoGr	11	8.8	8.8
β TCLA	W	5	12.6	12.6
β TCLD	W	3	21.0	35.1
δ TCP	CFC	1	10.8	18.7
δ TCSG	MoGr	4	13.0	21.7
δ TCLA	W	5	14.4	24.1
δ TCLD	W	4	21.0	35.1
TCT	W	12	14.0	10.5
experimental TCLD	W	8	21.0	35.1
TCDQ	CFC	1	9.8	9.8
extraction TCLA	W	2	11.8	11.8
extraction TCLD	W	1	21.0	35.1

Table 1: The FCC-hh collimator materials, numbers (per beam), and settings throughout the cycle. The settings are given for the reference value of 2.2 µm of the normalized emittance.

After initial simulation results, the design diverged from the LHC system, which has three betatron TCPs (in the horizontal, vertical and skew planes). Initial energy deposition simulations showed that the power load from secondary particles on the skew TCP was too high. The collimator would have been unlikely to survive. To achieve acceptable power loads, some changes have been done to the collimator materials and design. The length of the primary betatron collimators has been reduced to 30 cm from 60 cm and their thickness has been increased from 2.5 cm to 3.5 cm. This reduces the power load inside the collimator jaws and support structure. Removal of the skew TCP allows the secondary particle showers to expand and reduce their energy density. The subsequent collimator that these secondary particles will hit is the first secondary collimator. The initial energy deposition simulations found that the secondary particles would not directly hit the collimator jaw, but the mounting mechanism behind it. Because of this, the thickness of the jaws of the first secondary collimator has been increased from 2.5 cm to 4.5 cm.

Particles interacting with the collimation system can lose energy, but survive and exit the collimation region. Following the collimation insertions, the dispersion is matched to that of the arc region in the DS. Inside the DS, the dispersion rapidly rises. Any sufficiently off-momentum particles will impact the beam pipe aperture due to the dispersion. This will quench magnets if dedicated protection is not installed. Because of this, DS collimators, known as TCLDs are

installed in this region specifically to catch these off-momentum particles, as planned for HL-LHC [15]. Each experimental IR has 2 sets of TCLDs installed, and due to the higher particle load in the collimation regions these have additional TCLDs. In the betatron insertion, 3 TCLDs are used, and in the energy collimation, 4 are used. In addition, due to optical changes between injection and collision, the peak dispersion position changes between the injection and collision optics. The additional TCLD (over the HL-LHC number) is also required to cover both the injection and collision case.

In the experimental straight sections, it was found that one set of TCT collimators was insufficient. Beam losses were found to take place both inside the matching section, and also between D1 and D2. An extra pair of TCT collimators were installed in the matching part of the straight section, in order to catch these losses. This should also reduce experimental backgrounds.

For the extraction insertion, debris from the extraction protection (TCDQ) was found to impact the beam pipe at the end of the straight section. The level of losses in this region was found to be excessive for a 12 min BLT. To protect the machine, an extra pair of TCLA type collimators were added in the straight section after the TCDQ; one in the horizontal and one in the vertical plane. In addition, a TCLD type collimator was added at the start of the arc, which provides additional protection in case of a failure of the dump system.

3 MACHINE APERTURE

For the collimation system to work properly, it must be ensured that the beam-stay-clear around the FCC-hh ring is sufficient. This is usually most critical at injection energy, where the geometric emittance is larger. Aperture bottlenecks could also arise in the inner triplet at top energy, when the β-functions are squeezed at the collision points.

To study the available aperture, we use the same approach as for the LHC and HL-LHC [20, 21, 22]. The aperture module of MAD-X [23] is used to quantify the smallest distance, in units of beam σ, between the beam centre and the mechanical aperture that is found anywhere on the 2D cross section of the beam screen. The calculations are performed at several longitudinal locations in each element in order to obtain the minimum beam-stay-clear as a function of s. Various imperfections are included: a radial closed orbit offset $x_{\rm co}$, a fractional change k_β in beam size from β-beating, a momentum offset δ_p, and a relative parasitic dispersion $f_{\rm arc}$ coming from the arc.

The values assumed for these tolerances are shown in Table. 2. Since it is very hard to accurately estimate these for FCC-hh, they have been derived from the HL-LHC assumptions [20, 21, 22], which in turn have been shown to be pessimistic compared to the aperture measurements performed in the LHC [24, 25, 26, 27, 28, 29, 30, 31, 32, 33]. It should be noted that the values of the momentum offsets are pessimistic compared to the calculated RF bucket height. This gives a small additional safety margin, however, it should be noted that these values may change in the future. Mechanical and alignment tolerances are not well known for the FCC magnets at this stage and the HL-LHC values are used as working assumptions.

The last line of Table 2 shows the protected aperture, i.e. the smallest calculated aperture that is allowed in any machine element. This values has, as working assumption, been re-scaled from HL-LHC by the ratio of the square-root of the emittances. This assumption is, however, not

PRELIMINARY COLLIMATION
SYSTEM DESIGN CONCEPT AND
PERFORMANCE ESTIMATE

EuroCirCol-P3-WP2-
D2.6, EDMS
2041777

Date: 27/02/2019

trivial and needs to be studied in greater detail. The value of the protected aperture depends on the distribution and intensity of the halo that escapes the collimation system, as well as the halo that escapes the protection devices during failures, which are combined with detailed knowledge on the quench limit and damage limits of the machine elements [21]. Such studies have have not yet been performed in detail for the FCC and, pending them, the HL-LHC parameters are assumed.

Table 2: The parameters used in the MAD-X model for FCC-hh aperture studies at top energy and injection.

Parameter set	FCC-hh injection (3.3 TeV)	FCC-hh top energy (50 TeV)
Primary halo extension	$6\,\sigma$	$6\,\sigma$
Secondary halo, hor./ver.	$6\,\sigma$	$6\,\sigma$
Secondary halo, radial	$6\,\sigma$	$6\,\sigma$
Normalised emittance ϵ_n	$2.2\,\mu$m	$2.2\,\mu$m
Radial closed orbit excursion x_{co}	2 mm	2 mm
Momentum offset δ_p	6×10^{-4}	2×10^{-4}
β-beating fractional beam size change k_β	1.05	1.1
Relative parasitic dispersion f_{arc}	0.14	0.1
Protected aperture (σ)	13.4	15.5

In the calculations, the present design of the arc beam screen as of July 2018 has been adopted, as shown in Fig. 5. It should be noted that all arc dipoles are straight, which gives rise to a reduction in aperture due to the sagitta. This aperture reduction has been pessimistically modelled as a constant decrease of mechanical aperture of half of the sagitta on each side of the beam screen all along the length of the magnets. A sagitta of 2.524 mm was used for the aperture calculations. About 0.6 m downstream of every arc dipole a synchrotron radiation absorber protects the interconnection to the next magnet (see [34, Section 3.3.2]). While dimensions of the inner chamber of this absorber are the same as for the beam screen, the slits are not as deep and the sagitta is larger due to the longer distance from the dipole centre, resulting in a horizontal aperture reduction of 1.630 mm at the absorbers.

Several assumptions had to be made on the mechanical aperture, in particular that similar tolerances on manufacturing and alignment apply as in the LHC [35]. The FCC-hh arc beam screen in Fig. 5 features antechambers to channel synchrotron radiation. This was considered unnecessary for the straight section magnets, thus a scaled LHC-like beam screen design with a larger free aperture was assumed. Some detailed studies are required to determine whether this is justified for straight section magnets close to the arcs that might still receive some synchrotron radiation. The aperture tolerances were adapted from LHC elements. The beam screens in the warm sections for collimation and extraction should also be reviewed.

Using the parameters in Table 2, the aperture around the FCC-hh was evaluated at injection and top energy using the optics version 10. The results show that the full ring, including the
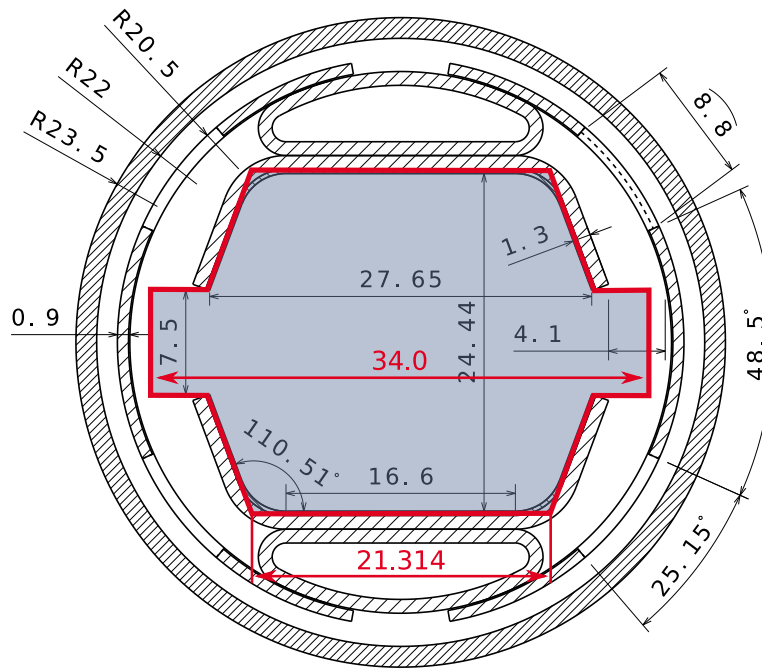
PRELIMINARY COLLIMATION
SYSTEM DESIGN CONCEPT AND
PERFORMANCE ESTIMATE

EuroCirCol-P3-WP2-
D2.6, EDMS
2041777

Date: 27/02/2019

Figure 5: The transverse cross section of the arc beam screen, the MAD-X model for the aperture calculations is outlined in red.

triplets in front of the high-luminosity experiments, meets the criterion at top energy. The top-energy triplet aperture at the high-luminosity experiments in IRA and IRG is shown in Fig. 6 for ultimate optics with $\beta^* = 30$ cm, and it can be seen that there is still some margin left. This margin could potentially be used to squeeze the optics further down to around $\beta^* \approx 21$ cm. This includes an increased crossing angle to keep the normalized separation constant.
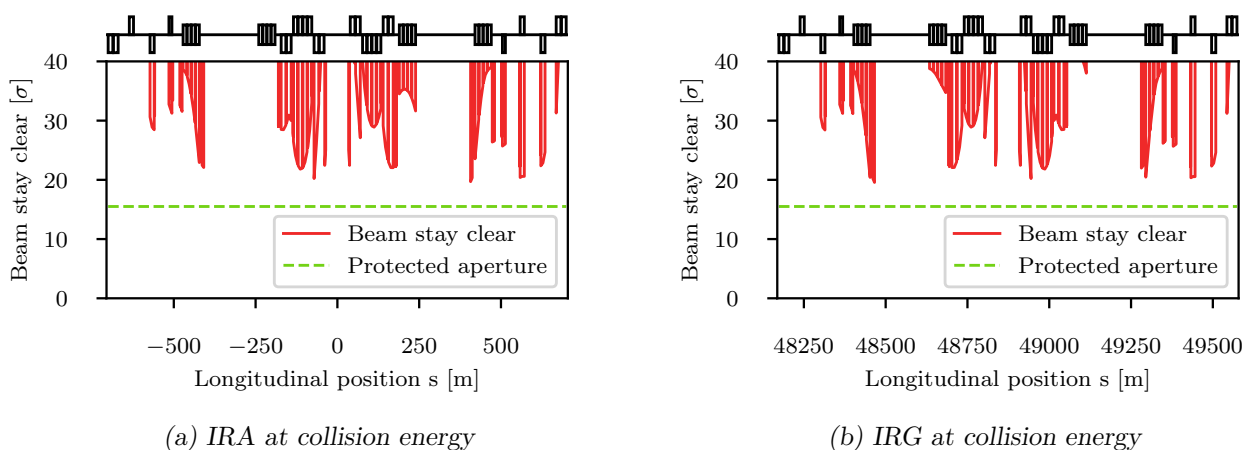

(a) IRA at collision energy

(b) IRG at collision energy

Figure 6: The calculated aperture at top energy, using the ultimate optics with β^* =30 cm, as a function of distance s in the high-luminosity experiments in IRA and IRG, shown together with the criterion for the minimum aperture.

PRELIMINARY COLLIMATION
SYSTEM DESIGN CONCEPT AND
PERFORMANCE ESTIMATE

EuroCirCol-P3-WP2-
D2.6, EDMS
2041777

Date: 27/02/2019

At injection, most elements around the ring are found within specification, in particular the arcs, in spite of the pessimistic modelling of the beam screen. An example is shown in Fig. 7. A few elements do not meet the criterion and have a too small beam-stay-clear. These are listed in Table 3. As can be seen, there are only three types of magnets affected: orbit correctors in the extraction and betratron collimation section (elements starting with MCB) as well as matching quadrupoles (MQMO) and tuning quadrupoles (MQTLH) of the betratron collimation section. Figure 8 shows the aperture bottlenecks in IRJ. The aperture issues of the MCB and MQMO magnets can simply be solved by replacing them with larger aperture magnets of the MCBY and MQY classes respectively. These magnet classes are already used in various locations along the ring and provide sufficient strengths. The MQTLH magnet issues also have to be solved for the final design but are not believed to be serious show-stoppers.

Previous lattice versions showed aperture limitations in the dispersion suppressors where the optics required a certain degree of freedom in terms of beam size but the aperture is given by the arc dipole design. Several mitigation measured have been proposed if these issues reemerge as the lattice evolves. One such measure involves pursuing the studies to refine the aperture criterion and the parameters in Table 2 and to investigate whether any of them can be improved. The mechanical tolerances on the manufacturing and alignment could possibly also be improved. In particular, in the few concerned locations, magnets could be installed that are better than the specification, either by sorting the magnets and simply taking the best ones among the full production, or by designing a special beam screen in these magnets only.
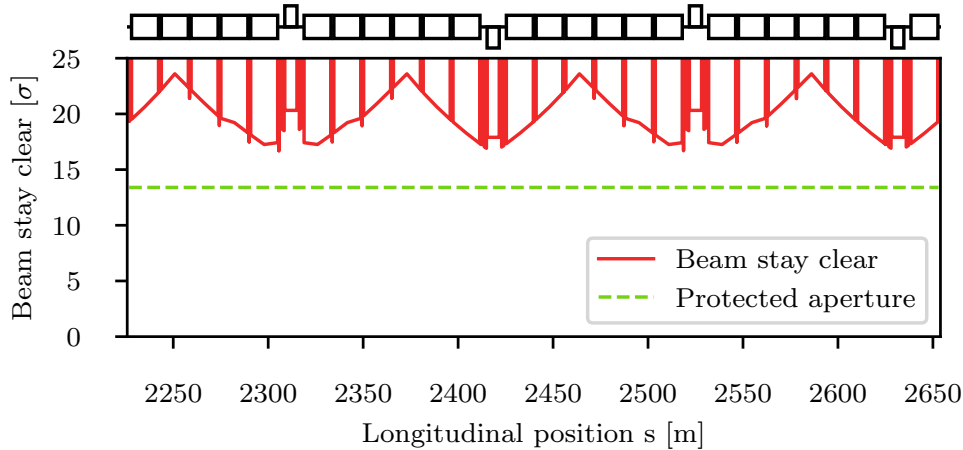

Figure 7: The calculated aperture at injection energy, as a function of distance s over two arc cells, shown together with the criterion for the minimum aperture.

In conclusion, using the preliminary aperture parameters that are taken over, or scaled from the HL-LHC, the vast majority of the elements around the FCC-hh ring meet the specification. While there are a few outliers, most of them can be cured by a simple switch of magnet type. For the the remaining ones in magnets of the MQTLH type, some further studies are needed on the element design, however, it is not believed to be a serious showstopper. The calculations should be repeated in the future using updated parameters specifically tailored to the FCC-hh.

PRELIMINARY COLLIMATION
SYSTEM DESIGN CONCEPT AND
PERFORMANCE ESTIMATE

EuroCirCol-P3-WP2-
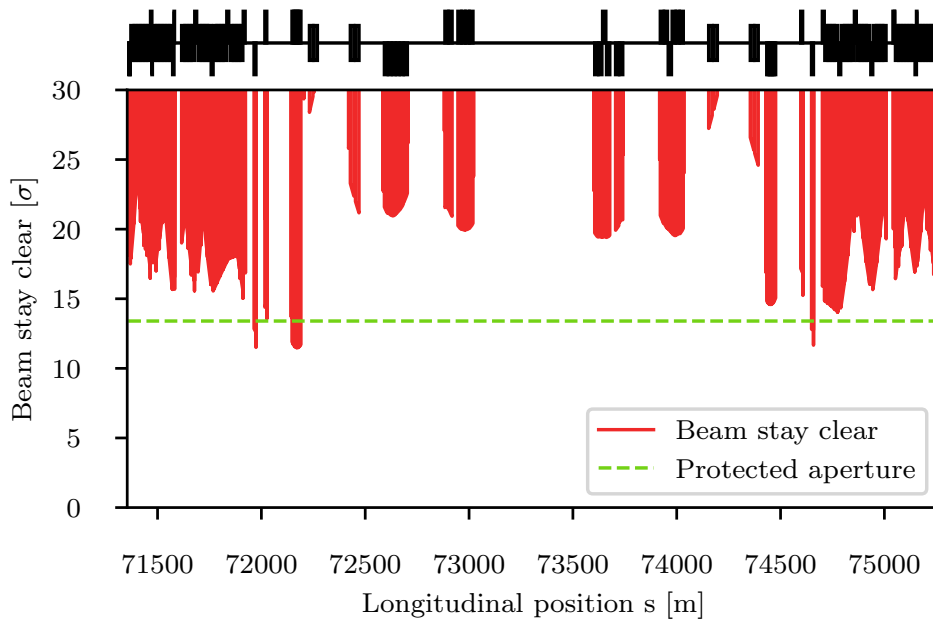D2.6, EDMS
2041777

Date: 27/02/2019

Figure 8: The calculated aperture at injection, using the standard injection optics with $\beta^* = 4.6$ m, as a function of distance s in IRJ (betatron collimation). It can be seen that a few elements in the dispersion suppressor fall below the criterion for the minimum aperture.

Table 3: Elements found below the minimum aperture at injection energy.

Element name	s-location (m)	Calculated aperture
MCBV.6RD.H1	25629	10.2 σ
MQTLH.[A-F]6LJ.H1	72169	11.5 σ
MCBH.6LJ.H1	71974	11.5 σ
MCBV.6RJ.H1	74659	11.7 σ
MCBH.6LD.H1	23254	12.5 σ
MQMO.6LJ.H1	71974	12.6 σ
MQMO.6RJ.H1	74658	12.8 σ

4   SIMULATIONS OF THE COLLIMATION SYSTEM PERFORMANCE

In order to evaluate the cleaning performance of the system, tracking simulations of the loss pattern around the ring are performed, which is the topic of this section. Different loss mechanisms are considered, and the output is used for further studies of energy deposition (in Sections 5–6) and the thermomechanical response (in Sec. 7).

During collisions, the beam is squeezed to a small size at the interaction point, and in doing so, the beam size is also blown up in the inner triplet magnets. These become the aperture restriction of the machine. At the same time, the crossing angle is enabled to prevent parasitic head on collisions and long range beam beam effects. This reduces the available aperture. For

the studies at top energy, this worst case for the aperture is the configuration that is simulated. Studies were also done at injection with un-squeezed optics, where the aperture restriction is in other regions of the machine, such as the arcs and dispersion suppressors. The optics parameters used in the simulations are summarised in Table 4, and the collimator settings in Table 1.

Parameter	Unit	Value
Optics version		9
Injection energy	TeV	3.3
Collision energy	TeV	50.0
Injection β^* (IPA,IPG)	m	4.6
Injection β^* (IPB,IPL)	m	27.0
Collision β^* (IPA,IPG)	m	0.3
Collision β^* (IPB,IPL)	m	3.0
Injection crossing angle (all)	µrad	0
Collision crossing angle (IPA,IPG)	µrad	100
Collision crossing angle (IPB,IPL)	µrad	26

Table 4: A table showing the FCC-hh optics configuration used in this work.

Additionally an asynchronous dump is simulated at collision energy. This is an accidental loss scenario, where the extraction kicker magnets do not fire at the correct time, or do not fire with sufficient strength, resulting in the beam not being fully extracted from the storage ring correctly.

4.1 SIMULATION METHOD

At both injection and collision, 3 possible beam loss scenarios are simulated. These are beam losses in the horizontal plane, vertical plane, and both planes simultaneously (referred to as skew). Simulations are carried out using the coupling [36, 37, 38] between SixTrack [39, 40, 12, 41] and FLUKA [42, 43], where the first code tracks the particles through the whole ring and the second describes their interactions in the collimator material, until they are lost in the latter by a nuclear inelastic reaction or they reach elsewhere the machine aperture boundary. This framework has been benchmarked against measurements with LHC beam losses, and the simulations agree well with the measurements [44].

The input beam distribution corresponds to a given loss scenario, while the output gives two components. The first is the energy deposited into each collimator. In addition, the full phase space and location of each particle is dumped if it touches the beam pipe aperture. These particles are considered to be lost. These losses are then histogramed together to produce what is called a loss map. This shows the loss locations around the ring. For this work a longitudinal binning size of 10 cm is used.

In the FLUKA coupling framework, only positively charged stable baryons are tracked around the ring - e.g. protons, and heavy ions. All other particles are killed and are not tracked - their energy is considered to be lost in the collimator or shortly after. An energy cut of 30% was used in FLUKA for this work, meaning that particles below 70% of the initial energy are killed.

In analogy to Ref. [9], the cleaning inefficiency is defined as

$$\eta_c(s) = \frac{E(s)}{E_{tot}\Delta s}, \tag{1}$$

where η_c is the cleaning inefficiency, Δs is the longitudinal binning size (10 cm in this work), E is the energy that impacts the physical aperture in a given bin, and E_{tot} is the total energy deposited in the full simulation (including inside collimator jaws). The required value of η_c that keeps all magnets below quench level depends on the loss scenario and beam energy

4.2 BETATRON CLEANING

To study the betatron cleaning performance, where the halo is assumed to impact on the primary betatron collimators, a ring of particles is generated in the phase space of the collimation plane (e.g. x,x', y,y') with sufficient amplitude to just touch the primary collimator jaw, usually a with a flat distribution between 7.57 and $7.570001\,\sigma$ for a primary cut at $7.57\,\sigma$. There is no amplitude in the vertical or longitudinal plane; particles are injected on the reference orbit.

The halo, usually containing 100 million particles and generated at IPA, is then tracked for 200 turns, which is sufficient for most particles to be lost on a collimator in an inelastic interaction, or the physical beam pipe aperture.

To calculate the required cleaning performance, a quench limit of 10 mW/cm^3 is conservatively assumed for a continuous power load into the magnet coils at 50 TeV, in accordance with the magnet design assumptionsThis is slightly higher than the design assumption for the LHC magnets at 7 TeV [45], but it should be noted that recent studies of Nb3Sn magnets have shown significantly higher quench limits [46]. The losses at quench can then be calculated to 2.2×10^5 p/m/s by scaling the LHC design loss rate at quench (7.8×10^6 p/m/s [11]) by a factor 35, which is the estimated increase in energy deposition per proton at 50 TeV compared to 7 TeV [47]. Finally, assuming an instantaneous loss rate corresponding to a 12 minute BLT and full intensity, a maximum allowed cleaning inefficiency of $\eta_{c,\max} = 3\times 10^{-7}$/m is found. Similarly, for a 12 minute BLT at injection energy, the quench limit is estimated to $\eta_{c,\max} = 3 \times 10^{-5}$/m.

The simulated betatron cleaning at injection is shown in Fig. 9–11. The highest losses around the ring stay well below $\eta_c = 10^{-5}$/m and are thus considered safe.

The estimated losses at collision are shown in Fig. 12–14. This is considered the most critical scenario. It can be seen that also in this case, the cleaning inefficiency around the ring is below the estimated quench limit of $\eta_{c,\max} = 3 \times 10^{-7}$/m, which means that for a perfect case, the collimation system should be able to protect the cold aperture even in the rather demanding scenario for a 12 minute BLT. The shown results are for a horizontal beam halo but the results are not substantially different for vertical losses.

With the removal of the skew TCP from the layout, the skew beam halo at collision provides an interesting test of the performance of the system with this updated layout. Figure 16 shows losses in the betatron collimation insertion with the skew primary removed, for a halo with equal horizontal and vertical amplitudes. Instead of impacting a TCP, the beam first impacts the less robust TCSs. From a cleaning perspective, the performance is kept; the losses into the cold regions of the machine are not excessive thanks to the TCLDs, although significant losses appear downstream of IPA. A potential concern for these losses is the robustness of the skew secondary collimators. From LHC operational experience, skew losses are very rare. The

**PRELIMINARY COLLIMATION
SYSTEM DESIGN CONCEPT AND
PERFORMANCE ESTIMATE**

**EuroCirCol-P3-WP2-
D2.6, EDMS
2041777**

Date: 27/02/2019

Figure 9: Image showing the full ring lossmap at injection for a horizontal beam halo.
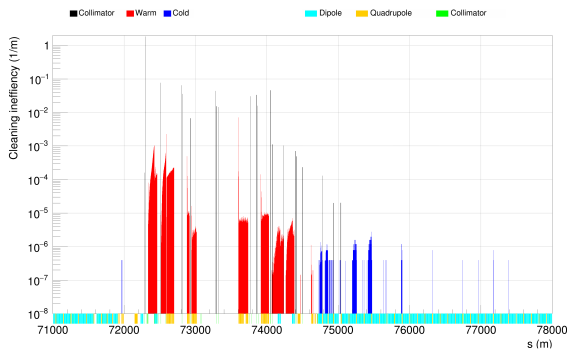

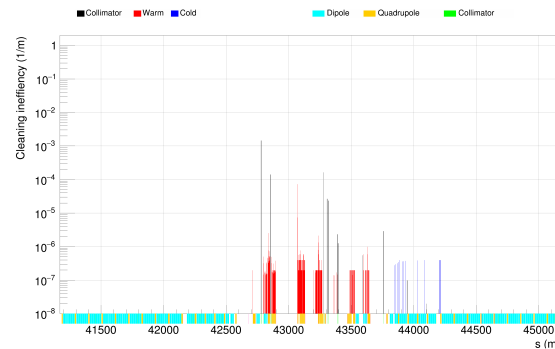*Figure 10: Image showing the betatron collimation insertion lossmap at injection for a horizontal beam halo.*

Figure 11: Image showing the energy collimation insertion lossmap at injection for a horizontal beam halo.

solution is to place a stricter limit on the BLT due to losses in the skew plane, consistent with the damage limit of the TCSs and the LHC operational experience.

4.3   OFF MOMENTUM BEAM HALO

For off-momentum losses, we study first the cleaning efficiency at the start of the ramp. The losses from un-captured beam at the start of the acceleration are simulated by injecting a pencil beam of off-momentum particles without betatron amplitude but with a δ_p/p such that they just impact the primary momentum collimator jaw (an energy of 3294.8025 GeV is used instead of the reference 3300.0 GeV).

**PRELIMINARY COLLIMATION
SYSTEM DESIGN CONCEPT AND
PERFORMANCE ESTIMATE**

**EuroCirCol-P3-WP2-
D2.6, EDMS
2041777**

Date: 27/02/2019

Figure 12: Image showing the full ring lossmap at collision for a horizontal beam halo.
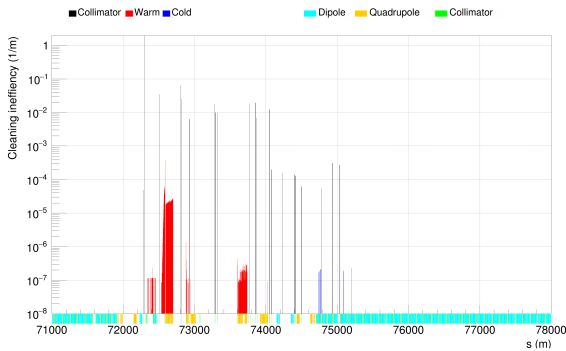

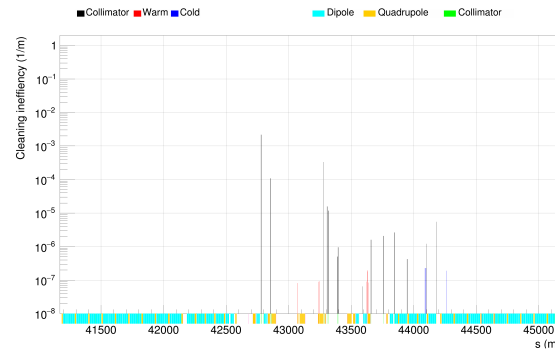*Figure 13: Image showing the betatron collimation system at collision for a horizontal beam halo.*

Figure 14: Image showing the energy collimation system at collision for a horizontal beam halo.

The resulting losses are shown in Fig. 18. Assuming a 1% beam loss over 10 s, the instantaneous lifetime is about 17 minutes, which requires the inefficiency to stay below $\eta_{c,\max} = 4 \times 10^{-5}$/m. As can be seen, all losses fulfil the criterion with some margin.

In collision, off-momentum losses can also be caused by uncaptured beam, but these losses are expected to occur at a slow steady rate, and not as a brief impulse. Therefore the cleaning criterion is not as strict as for the betatron case, where faster losses are more likely. Irregular losses could be faster, e.g. during a fault of the RF system, however, such events are expected to be very rare. Dedicated simulations are needed to quantify a limit on the allowed loss rate from off-momentum halo at collision energy.
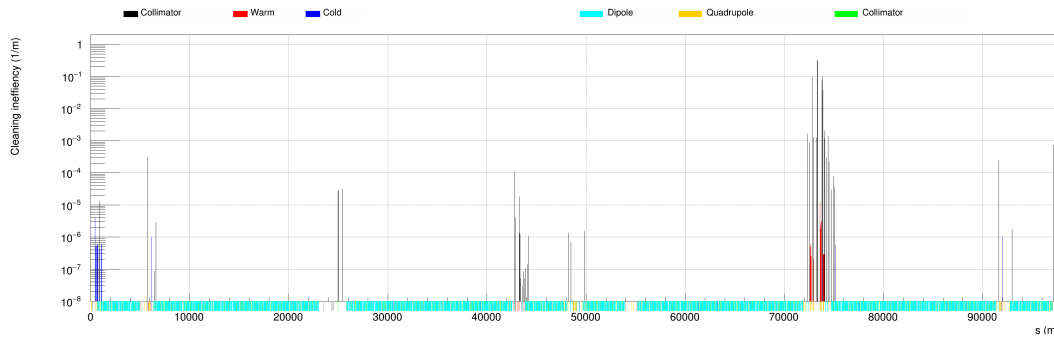
Figure 15: Image showing the full ring lossmap at collision for a skew beam halo.
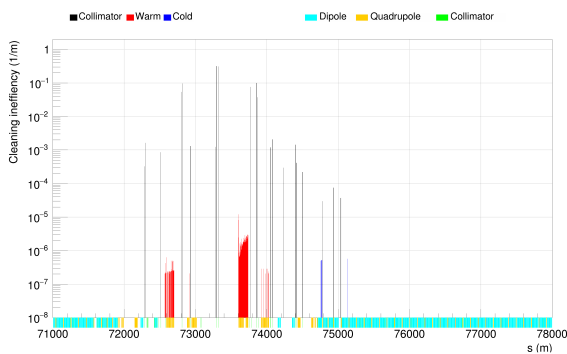

Figure 16: Image showing the betatron collimation system at collision for a skew beam halo.
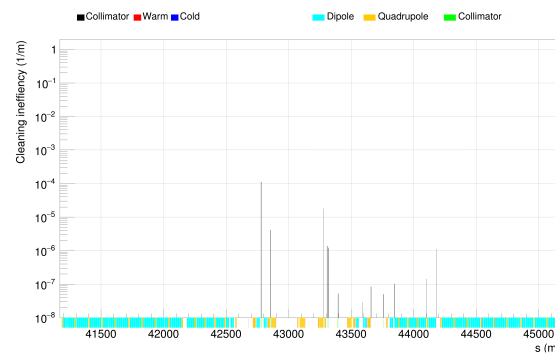

Figure 17: Image showing the energy collimation system at collision for a skew beam halo
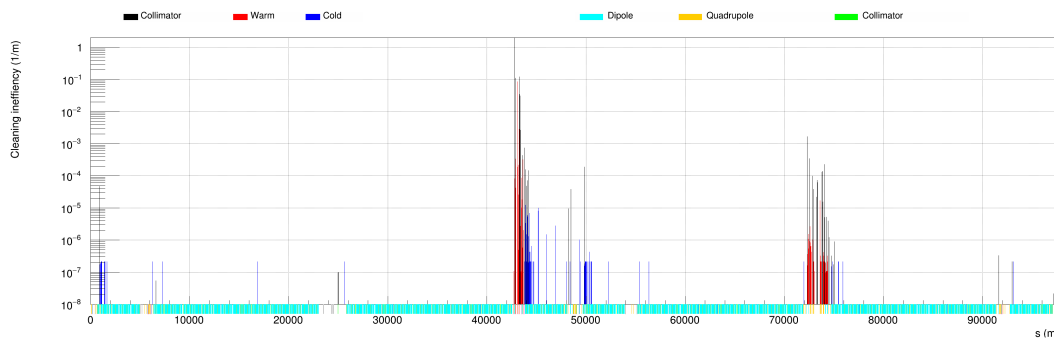

Figure 18: Image showing the full ring lossmap at injection for an off momentum beam halo.

4.4   ASYNCHRONOUS BEAM DUMP

One possible failure scenario is that of the asynchronous beam dump. Here, one or more extraction kicker could pre-fire asynchronously to the abort gap and hence cause an erronous deflection of the circulating beam. This could result in the beam not being correctly extracted from the storage ring to the beam dump. In case of the LHC, such a failure would almost immediately re-trigger the remaining extraction kickers. Nevertheless, in an extreme case, the beam risks
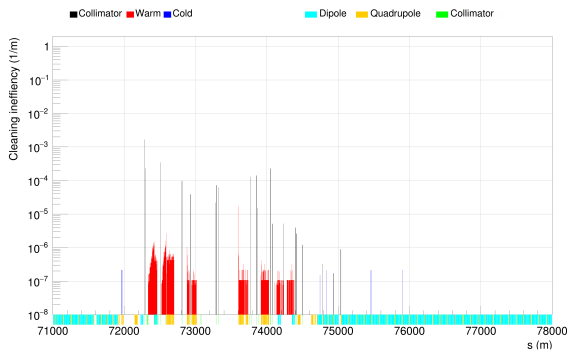
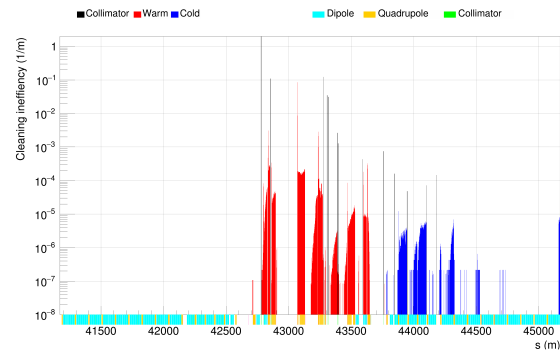*Figure 19: Image showing the betatron collimation system at injection for an off momentum beam halo.*

Figure 20: Image showing the energy collimation system at injection for an off momentum beam halo.

impacting the machine aperture. For FCC-hh, the proposed alternative abort strategy proposes a delayed synchronous beam dump, resulting in part of the mis-kicked beam oscillating for one additional turn.

Dedicated collimators (TCDQ), as well as septum protection (TCDS), are in place to protect against mis-kicked beam. However, beam could leak out of the TCDQ or pass it in case of an error on the TCDQ position, or potentially sensitive collimators or aperture bottlenecks could due to errors arrive at effectively smaller apertures than the TCDQ. The collimation system should be able to survive such an accident.

In the version of the FCC used, the extraction takes place in the horizontal plane, and the system uses 300 segmented kicker magnets. It should be noted that a newer version exists, where the extraction is instead vertical, and that these studies should be redone for that case. The goal of this study was to obtain the maximum number of kicker magnets that could fire at the same time before damage occurs at a collimator.

In the simulation, the beam was tracked for 1 turn, n extraction kickers were enabled on turn 2, the beam was then tracked for one further turn and extracted. The initial conditions are for a full beam, including also the core. The distribution corresponds to the sum of two gaussians: The core consists of 95% of particles, with a 1σ standard deviation, while the halo makes up the remaining 5%, with a 1.8σ standard deviation as from the Van der Meer scans in Ref. [48]. Particles are generated up to the TCP cut.

The resulting losses, for different number of kickers firing and normalized to the absolute number of impacting protons, are shown in Fig. 21–24. This can be compared to an estimated damage limit of 1×10^{11} protons. From the plots, it can be seen that up to 3 kickers can fire safely. For more than 3 kickers, e.g. 4 or 5, it can be seen that this is potentially not safe. The updated layout of the extraction insertion comprises 150 kicker magnets instead of 300. Furthermore, considering the impact of the updated optics with a vertical kick the limit would be reduced to just 1 kicker pre-firing. For final conclusions, studies on the influence of imperfections on the TCDQ position should also be carried out.

Figure 21: Image showing the loss distribution with 1 extraction kicker pre-firing.
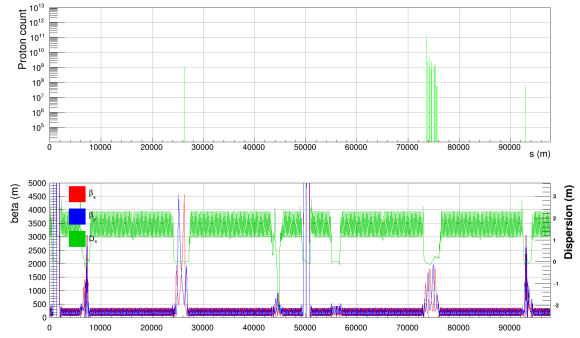

Figure 22: Image showing the loss distribution with 3 extraction kickers pre-firing.

Figure 23: Image showing the loss distribution with 4 extraction kickers pre-firing.

Figure 24: Image showing the loss distribution with 5 extraction kickers pre-firing.

4.5 INFLUENCE OF IMPERFECTIONS

The results of previous sections refer to an ideal machine. In reality, unavoidable imperfections of the collimators and the rest of the machine affect the cleaning performance of the collimation system. In order to evaluate their influence, several cases with combined imperfections have been simulated. The error model is introduced in SixTrack following the procedure and experimental data used for the LHC [11, 12]:

1. Imperfections of the jaw flatness can reduce the length of material seen by the impacting protons. The jaw flatness error is modelled by a second order polynomial applied over a number of slices:

$$\pm 4 \cdot 10^{-4} (\frac{s^2}{l} - s) [m] \tag{2}$$

   where s is the longitudinal position along the jaw and l is the jaw length in m. In this study four slices are used with the deformation bent outwards the beam as shown in Fig.25.

2. The beam orbit and center of the collimator gap are not always perfectly aligned, which were modelled through random offsets of the centers of collimators with a standard deviation of 100 μm (see Fig. 26).

PRELIMINARY COLLIMATION
SYSTEM DESIGN CONCEPT AND
PERFORMANCE ESTIMATE

EuroCirCol-P3-WP2-
D2.6, EDMS
2041777

Date: 27/02/2019

3. Angular misalignments of the collimator jaws with respect to the beam axis are added with an rms tilt angle of 200 μrad (see Fig. 26).

4. Random errors on collimator gaps were applied with a standard deviation of 0.17 σ, corresponding to an rms β-beating of 4% as assumed for FCC-hh [49].

5. Tolerances of aperture misalignments for the different type of magnets are used to introduce imperfections in the alignment of the accelerator elements.
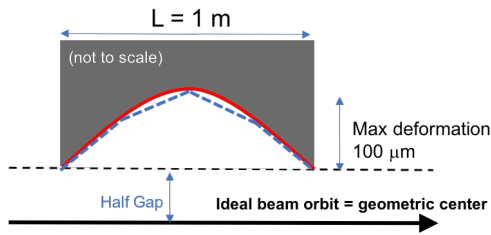

Figure 25: Jaw deformation for 1 m long collimator modelled by a 2nd degree polynomial in red and the 4 slices approximation used in SixTrack in dashed blue.
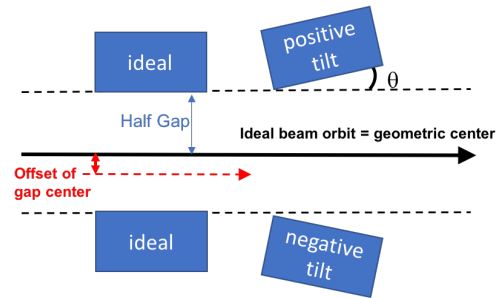

Figure 26: Illustration of the various errors applied to collimator in simulation.

A full study of optics imperfections, adding magnetic and alignments errors in the lattice through MAD-X and partially correcting them to get a realistic β-beating and orbit, has not been performed but is foreseen as future work. Phase advance and dispersion beating can only be introduced with this second method. Apart from the jaw flatness error, all the imperfections follow a Gaussian distribution cut at 3 σ and are controlled by a seed. Twenty seeds are used for each scenario with combined imperfections. The number of seeds is limited by computational time, which represents several decades for this study.

The FCC-hh lattice used in this study is V9 for the beyond ultimate case with $\beta^* = 15$ cm at collision to investigate the most challenging scenario. The horizontal betatron loss maps have been simulated for multiple imperfection scenarios. The SixTrack version used for this study relies on the internal scattering module [40] and the cleaning inefficiency in the following plots represents the fraction of protons lost in a longitudinal bin normalised by the bin length ($\eta = N_{lost}^{\Delta s}/[N_{lost}\Delta s]$). The collimation system considered is the one of Table 1, however, in an earlier version with the skew TCP in IRJ still in and all the TCSs made of CFC. The length of the TCPs is 60 cm, the TCDQ is 10 m in length whereas other collimators are 1 m. The simulation setup is identical to the one in Sec. 4, but with an impact parameter of 0.0015 σ.

In Figs. 27–28 we present the loss maps for the ideal case and an example with all imperfections. As expected, most protons are lost in the collimation regions IRF and IRJ. These results allow us to predict where possible quenching events may occur, and give an indication about how to modify the collimator settings along the accelerator in order to improve the system performance. The loss map for the ideal machine in Fig. 27 shows very few cold losses compared with several blue spikes present in the loss map with imperfections. Most of the cold losses appear between the detector IRA and IRB, around the dump insertion region IRD and downstream the

**PRELIMINARY COLLIMATION
SYSTEM DESIGN CONCEPT AND
PERFORMANCE ESTIMATE**

**EuroCirCol-P3-WP2-
D2.6, EDMS
2041777**

Date: 27/02/2019

RF insertion IRH. The majority of loss maps with all imperfections activated show a similar behaviour.
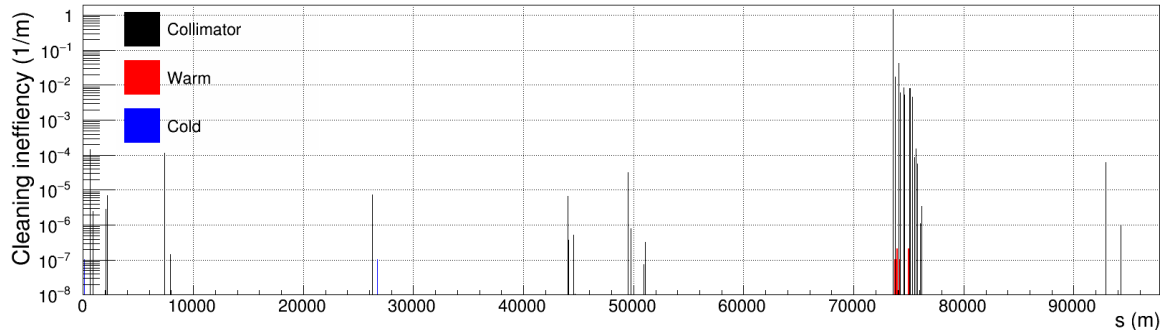

Figure 27: Horizontal loss map for the ideal case without imperfections.
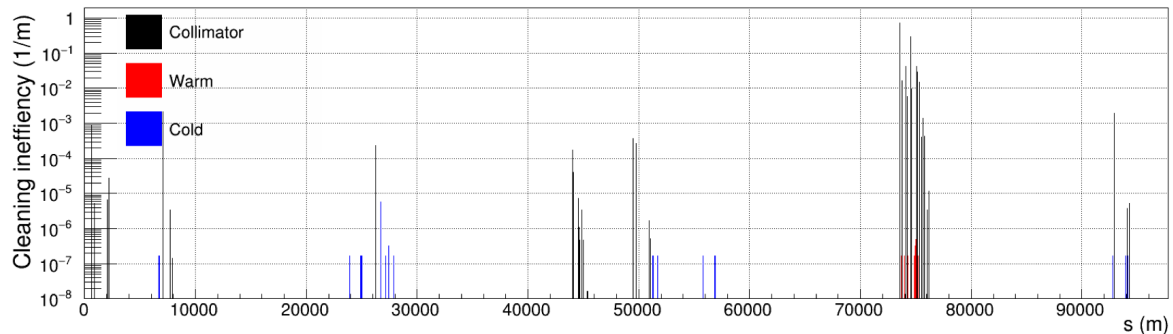

Figure 28: Example of horizontal loss map with all imperfections considered.

The influence of different imperfection types on the losses on collimators is summarised in Fig. 29 where ratio of losses on different collimator families to the TCP losses is presented. In the horizontal axis the different cases are indicated starting from the ideal case and then adding the imperfection types in steps. Each point represents an average over the 20 seeds with their standard deviation. For all cases the ratio below one indicates that no hierarchy breaking has been observed in simulations, including the error bars. For TCLAs, TCDQ, and TCLDs, a slight increase can be observed with wider error bars. In Fig. 30, we present the ratio between the TCT losses and the TCP losses. In this case, the TCT losses increase as more imperfections are included. It can be seen that with all imperfections losses in tertiaries are about 4 times higher with respect to the ideal case, which could have a potential on the machine-induced background.

The warm and cold global inefficiencies, defined as the sum of all inefficiencies in warm and cold apertures of the machine, are shown in Fig. 31. The changes to the global inefficiency for warm elements is within the error bars. For cold elements an increase of factor 2 with respect the ideal case is observed after introducing offsets errors of the collimator gaps. Including tilt errors, the global inefficiency is about a factor 5 higher than in the ideal case, while adding gap and flatness errors gives as final increase a factor of about 6.

The highest cold losses in a single 10 cm bin is presented in Fig. 32. Most of the simulations with imperfections show an almost complete loss of all protons (more than 95%). For the ideal
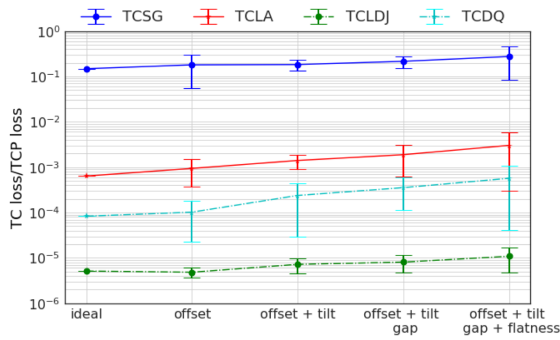
**PRELIMINARY COLLIMATION
SYSTEM DESIGN CONCEPT AND
PERFORMANCE ESTIMATE**

**EuroCirCol-P3-WP2-
D2.6, EDMS
2041777**

Date: 27/02/2019

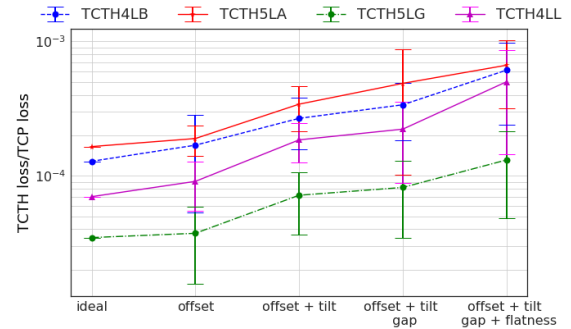*Figure 29: Influence on different collimator losses as simulated by SixTrack.*

Figure 30: Influence on different tertiaries collimator losses as simulated by SixTrack.

case the number of simulated protons was increased to 140M to get a similar amount of total losses and a comparable η_c for a loss of a single particle in the simulation. Fig. 32 indicates that on average only a single proton is lost in a single longitudinal bin for the ideal case and for the offset-tilt cases. When adding gap errors and flatness imperfections the inefficiency in a single location increase up to 3 times the single event inefficiency, however, most seeds stay within the estimated requirement of $\eta_{c,\max} = 3 \times 10^{-7}/\mathrm{m}$, which gives confidence in the system performance. For the ultimate optics case of this study, the highest cold peak increases by a factor 2 on average and the global cold inefficiency by a factor 4.
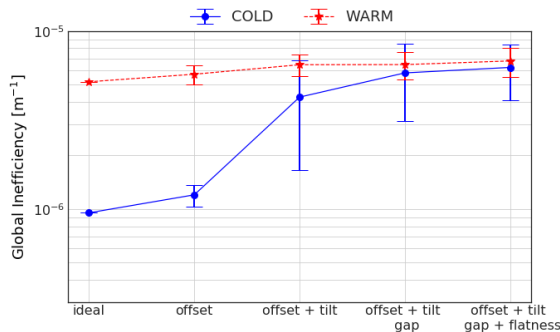

Figure 31: Global cold inefficiency calculated as sum of all cold imperfections for all combined scenarios.
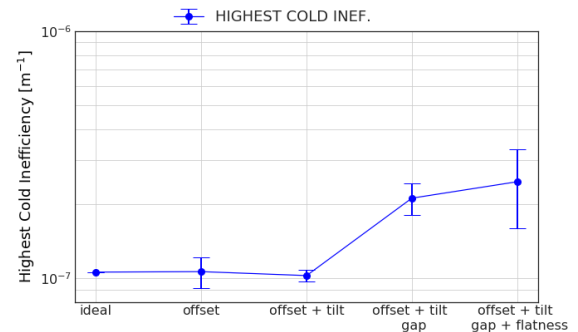

Figure 32: Highest cold inefficiency in a single longitudinal bin of 10 cm for different combined scenarios.

5   ENERGY DEPOSITION IN COLD MAGNETS

The tracking simulations described in the previous sections give as output the distribution of protons lost on the apertures around the ring. Based on this, an approximate estimation were made on whether the protection of the cold aperture is adequate. For a detailed assessment of particularly critical locations, it is required to perform local energy deposition studies. In particular, the impacts on the collimators cause secondary particle showers that are not evaluated in the tracking simulations and which can extend into neighbouring magnets. In this section

PRELIMINARY COLLIMATION
SYSTEM DESIGN CONCEPT AND
PERFORMANCE ESTIMATE

EuroCirCol-P3-WP2-
D2.6, EDMS
2041777

Date: 27/02/2019

we therefore examine the expected energy deposition in the dispersion suppressor of IRJ, which is the most critical cold part of the machine, and in particular in the cold magnets installed downstream of the TCLDs.

The Monte Carlo program FLUKA [42, 50] was used in order to evaluate the energy deposition in the cold region around a TCLD, downstream of the betatron cleaning insertion straight section [51]. The distribution of protons leaking out of the upstream betatron collimators at the start of cell 8 was used as starting conditions. They were extracted from tracking simulations carried out at 50 TeV using the MERLIN code [52, 53], and the FCC-hh lattice as of 2017 [54]. Only cell 8, including the TCLD, was simulated, in the assumption that the situation around the other TCLD in cell 10 would be similar or better. An identical result and mitigation strategy can thus be assumed for cell 10.

A 3D geometry of the region was implemented as shown in Fig. 33, including the TCLD and two downstream magnets (a quadrupole and a dipole). Since at the time of the study a detailed geometry of the dipole was not available, simplified models based on the current LHC magnets were used with the addition of the FCC coil design and beam screen [55]. Magnetic fields were included in both magnets, modelled as perfect quadrupolar or dipolar fields, extending over the vacuum chamber, beam screen and cold bore. The collimators were modelled as two parallel blocks of the tungsten alloy Inermet 180, including a tapering part. The masks were modelled as cylinders of the same material. Full details can be found in Ref. [51].

In the FLUKA simulations, typically 4×10^6 protons were simulated, and the energy deposition was scored in the coils of the dipole and quadrupole. To normalise the simulated energy deposition per lost proton, a 12 minute BLT was assumed for the nominal FCC-hh beam parameters at 50 TeV, with all losses impacting on the primary collimator, in order to obtain a power load in the superconducting coils.

For the studies, several layouts of TCLDs and masks were tested and iteratively adjusted until a satisfactory solution was found. The final proposed layout includes a main 1.0 m TCLD, followed by a second 1.5 m TCLD, and a 0.5 m mask in front of the dipole. An additional 1.5 m TCLD and a 0.15 m mask were placed in front of the dipole. For this layout, labelled "Updated design", the resulting energy deposition along the length of the coils of the quadrupole and dipole is shown in Fig. 34. For every longitudinal position, the figure shows the maximum over all bins transversely.

In the figure, the simulated power load has been scaled up by a safety margin of a factor 8. This factor includes both the effect of imperfections, not included in the tracking simulations used here, and the underestimation of the measured energy deposition found in previous studies [12], even after imperfections were included.

It can be seen in Fig. 34 that for a previous layout iteration consisting of only two 1 m TCLDs and a single mask, the power load exceeds the estimated quench limit of 10 mW/cm^3, while for the final layout with 3 TCLDs and two masks, it is well below. As noted before, this limit is likely pessimistic in view of the recent estimates of a 100-200 mW/cm^3 quench limit of the 11 T magnet [46], developed for HL-LHC and also based on Nb3Sn technology. This gives a significant safety margin in the final design, which based on these simulation results should be able to protect the cold aperture of the ring against quenches for a 12 minute BLT. Although these studies should be redone for the latest version of the FCC-hh lattice, which might cause minor layout changes, it is unlikely that the qualitative conclusions will change.

PRELIMINARY COLLIMATION
SYSTEM DESIGN CONCEPT AND
PERFORMANCE ESTIMATE

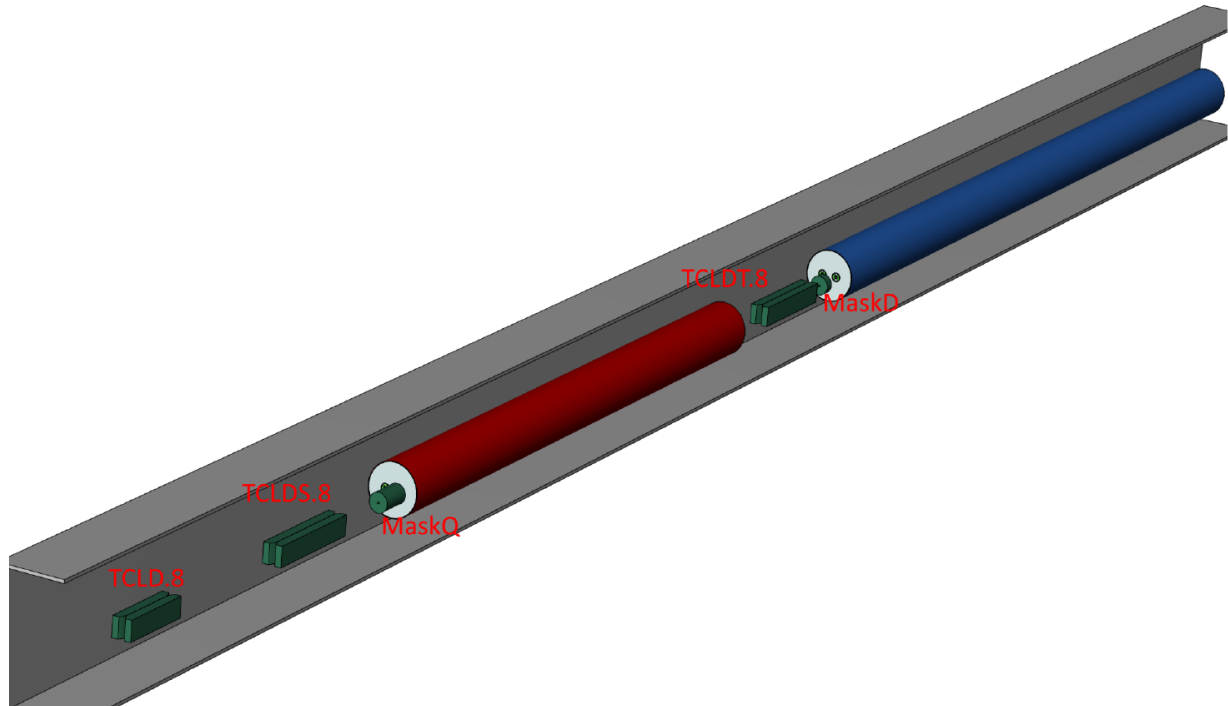EuroCirCol-P3-WP2-
D2.6, EDMS
2041777

Date: 27/02/2019

Figure 33: FLUKA geometry as implemented in cell 8 in the dispersion suppressor of IRJ, including three TCLDs and two fixed masks [51]. The collimators and masks are shown in green, the quadrupole in red, and the dipole in blue.
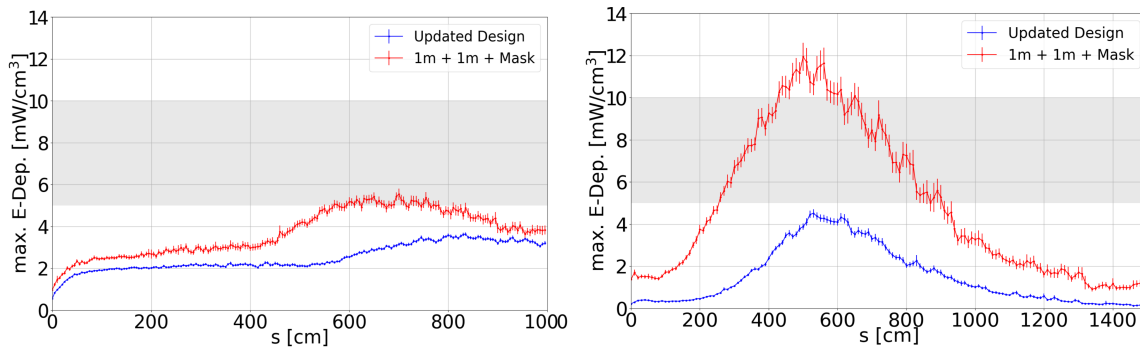

Figure 34: Peak power density along the quadrupole (left) and dipole (right) in cell 8 for the final protection design and the previous solution with the a factor 8 safety margin included [51].

6   ENERGY DEPOSITION IN WARM BETATRON SECTION

The power deposition is of high importance not only on the superconducting magnets, but also on the collimators themselves and on other elements in the warm section. The extreme load during a 12 minute BLT drop corresponds to a beam loss power of 11.6 MW, which is 24 times higher than for the nominal LHC and it should be sustained under up to 10 s. This represents a severe challenge for the robustness of the collimators and other exposed elements. Therefore, this section presents energy deposition studies of all elements in the warm section using FLUKA.

A cut of the initial part of the FLUKA model of the whole 2.7 km insertion is shown in Figure 35. An earlier version of the collimator configuration was used, which is identical to the one in Table 1 except that all TCSs are made of CFC. As in the LHC, three passive absorbers (TCAP), made of tungsten and copper, with lengths of 1.5 m, 0.4 m and 1 m, respectively, are placed in front of the most exposed magnets. Figure 36 shows the components of the collimator jaws as modelled, while a 3D view of a part of the tunnel is given in Figure 37.
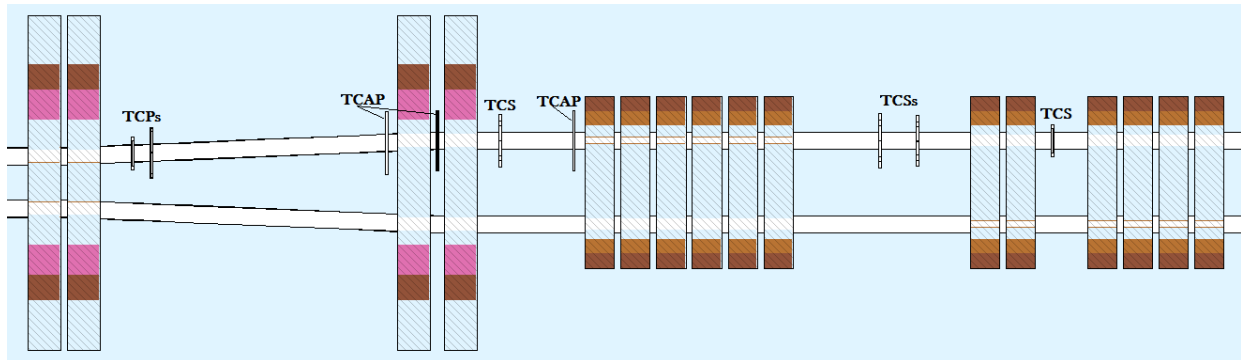

Figure 35: FLUKA model of the first 800 meters of the betatron collimation insertion.

In order to perform particle shower simulations and calculate energy deposition in the various beam line elements, maps of beam halo protons touching the collimator jaws are fed to FLUKA. These are produced by the above-mentioned online coupling between SixTrack and FLUKA. The relevant phase space details of each collimator hit is dumped as input for the second step of the simulation, performed by FLUKA only over its geometry model, as partially shown in Figure 35. Before being removed from the halo by either hitting the aperture or inelastic interactions inside a collimator, a halo proton touches the collimators on average more than once. Its hits are kept in the maps only if they occur in distinct turns, since possible multiple hits in the same turn are replicated in the course of the shower propagation.
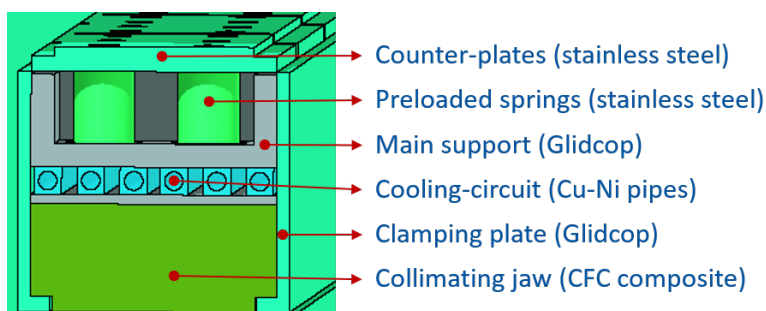
Figure 36: FLUKA model of a collimator jaw.

As a representative case, the vertical halo scenario, where hits are concentrated in the first TCP, was investigated through successive iterations. This case is more critical than horizontal losses, since the vertical TCP is most upstream and there is thus more distance within the section of the TCPs over which the shower can develop. In order to limit the power deposition on the jaws, three design measures were implemented. First, the TCP active length was halved with respect to the LHC (from 60 cm to 30 cm), this way reducing the shower development

**PRELIMINARY COLLIMATION
SYSTEM DESIGN CONCEPT AND
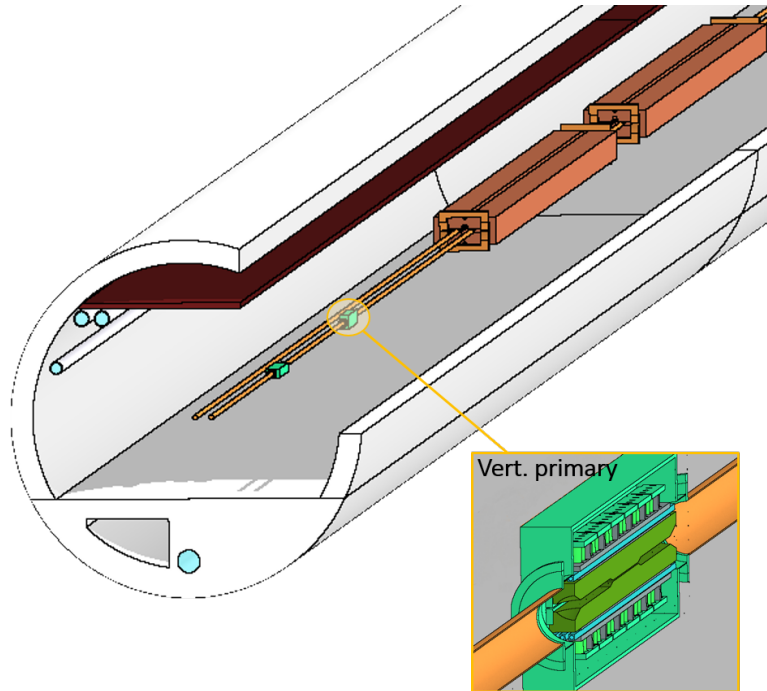PERFORMANCE ESTIMATE**

**EuroCirCol-P3-WP2-
D2.6, EDMS
2041777**

Date: 27/02/2019

Figure 37: 3D view of the FLUKA model of the Betatron cleaning insertion dogleg, hosting the primary collimators.

inside the absorbing material. Then the jaw thickness was increased (from 2.5 cm to 3.5 cm and 4.5 cm, for TCPs and TCSGs, respectively), since the metallic parts of the jaw cooling circuit turned otherwise out to be subject to the highest power density, being too close to the secondary particle shower core. Finally, the skew primary collimator, still collecting a total power significantly exceeding 100 kW for the design BLT of 12 minutes, due to its downstream position from the horizontal and vertical primaries, was removed.

The amount of the power deposition on the beam line elements and the infrastructure for the resulting configuration is reported in Figure 38. Almost half of the power is taken by the tunnel walls, while a significant fraction is absorbed by the beam pipes, along 2.7 km.

Table 5 details the loads on the collimation system elements. Among those in CFC, the first secondary collimator represents the most critical case. However, despite an integral load 14 times lower, the primary collimator directly impacted by the beam halo (TCP.D) is the one exposed to the highest power density, due to the multi-turn ionization by primary protons at extremely small impact parameters.

Figures 39 and 40 show the power density distribution in the vertical TCP. For the design BLT of 12 minutes, the maximum value is at 50 kW/cm^3 on the jaw surface layer, but 100 μm inside one already gets one order of magnitude less.

The horizontal TCP, which in the considered scenario is rather exposed to the particle shower from the upstream collimator, takes a total power 12 times higher than the latter, but its peak power densities are dramatically lower, up to 55 W/cm^3, albeit extended to a well larger area.

As pointed out above, the first TCS is affected by more severe conditions. Figure 41 illustrates the 3D distribution of its nearly 100 kW, showing also the picture obtained with the standard LHC jaw thickness of 2.5 cm that induces power density values up to 800 W/cc in the cooling
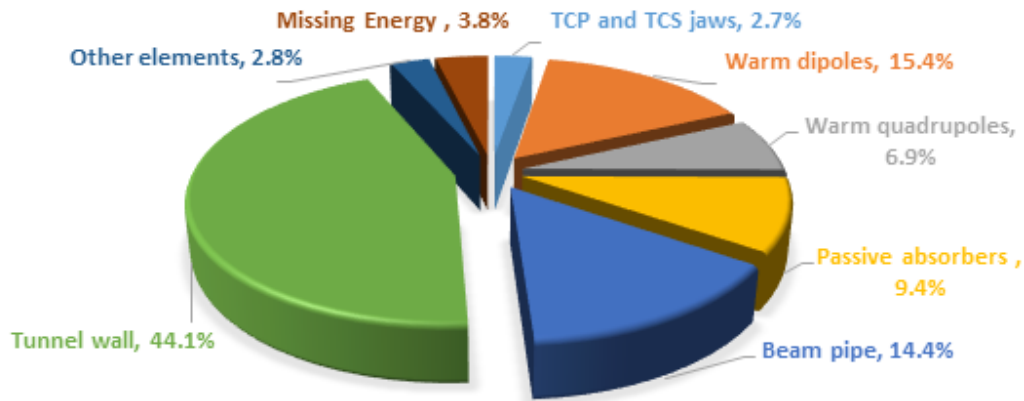
Figure 38: Power sharing in the betatron collimation insertion. The missing energy fraction refers to the energy spent in endothermic nuclear reactions as well as carried away by generated neutrinos.
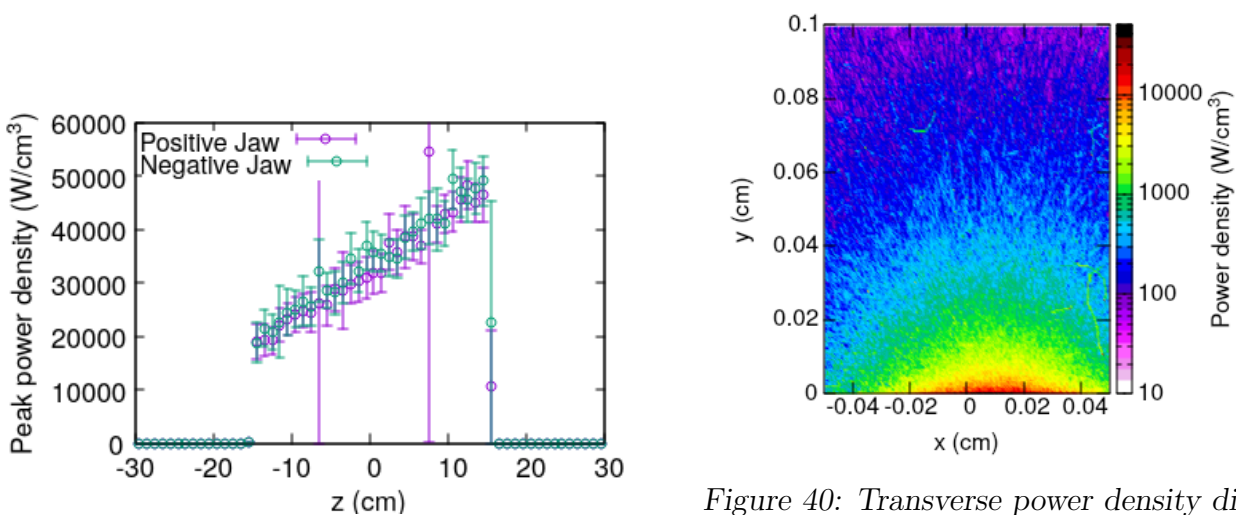

Figure 39: Peak power density profile along the length of the two jaws of the vertical TCP.

Figure 40: Transverse power density distribution in the most impacted area (1 mm x 1 mm) of the vertical TCP. The jaw surface is at y=0. Values are given for 12 min BLT, with a transverse (x/y) resolution of 5 μm and a longitudinal (z) resolution of 1 cm.

pipes and an integral load almost 2.5 times higher. With the proposed thickness increase to 4.5 cm, a maximum of 115 W/cc is found in the absorbing material. For the following collimators, this measure is less critical. Further studies of the thermo-mechanical response of the most critical collimators are shown in Sec. 7.

The two 17 m long warm dipoles that close the dogleg are particularly impacted, being exposed to the particle showers from the primary collimators. The second module, in the presence of the shortest passive absorber in front of it, collects more than 1 MW for a 12 min BLT. For reference, the LHC module, which is 5 times shorter, takes 22 kW assuming the same BLT with

PRELIMINARY COLLIMATION
SYSTEM DESIGN CONCEPT AND
PERFORMANCE ESTIMATE

EuroCirCol-P3-WP2-
D2.6, EDMS
2041777

Date: 27/02/2019

Table 5: Total power on collimators and absorbers for 12 min BLT

Primaries	Power (kW)
TCP.D6L	6.5
TCP.C6L	80
Scondaries	**Power (kW)**
TCSG.A6L	92
TCSG.B5L	9.8
TCSG.A5L	41
TCSG.D4L	33
TCSG.B4L	6.4
TCSG.A4L	12
TCSG.A4R	14
TCSG.B5R	3.3
TCSG.D5R	7.2
TCSG.E5R	12.5
TCSG.6R	2.3
Active absorbers	**Power (kW)**
TCLA.A6R	36.5
TCLA.B6R	2.0
TCLA.C6R	2.2
TCLA.D6R	1.6
Passive absorbers	**Power (kW)**
TCAPA.6L	545
TCAPB.6L	78
TCAPC.6L	484
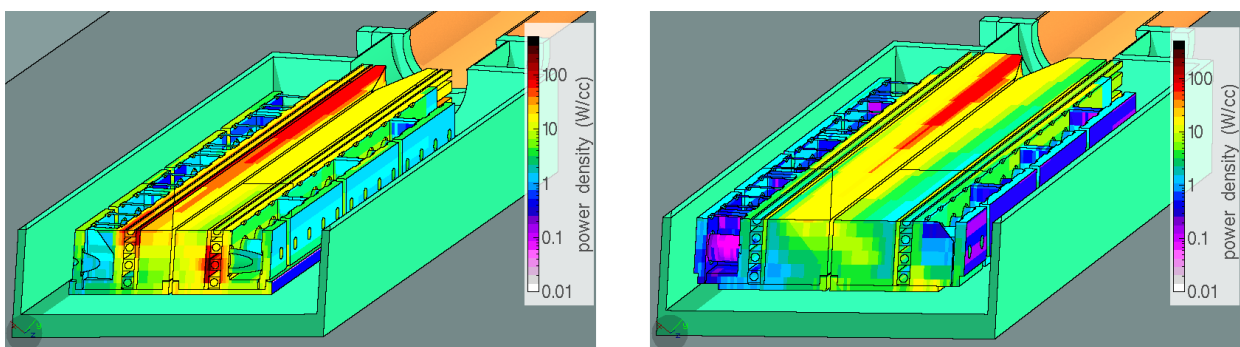
Figure 41: Power density distribution in the first secondary collimator for 12 min BLT.
Left: LHC jaw thickness of 2.5 cm. Right: proposed jaw with thickness of 4.5 cm.

nominal beam parameters. As shown in Figure 42, the MBW.A6 non-IP face reaches 270 kW/m,
while over most of its length the absorbed power is at about 60 kW/m, which translates into a
linear load from 10 kW/m to 100 W/m for more regular BLTs of 1 to 100 hours. This calls for a
suitable cooling system and a further optimisation of the front face protection, considering that

**PRELIMINARY COLLIMATION
SYSTEM DESIGN CONCEPT AND
PERFORMANCE ESTIMATE**

EuroCirCol-P3-WP2-
D2.6, EDMS
2041777

Date: 27/02/2019

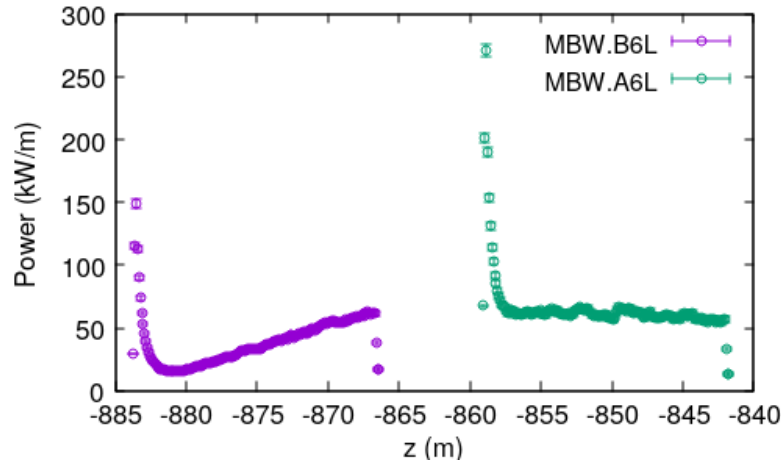the first meter of the magnet absorbs more than 10 % of the total power.

Figure 42: Integral power profile on the two warm dipoles after the primary collimators, for 12 min BLT.

Looking at the dose accumulated in the coils, it is clear from Fig. 43 that a critical gain is provided by the mechanical design, where the return coils are kept as far as possible from the beam pipe. If the LHC design would have been kept, with return coils closer to the beam, a one order of magnitude higher localised peak dose is expected.
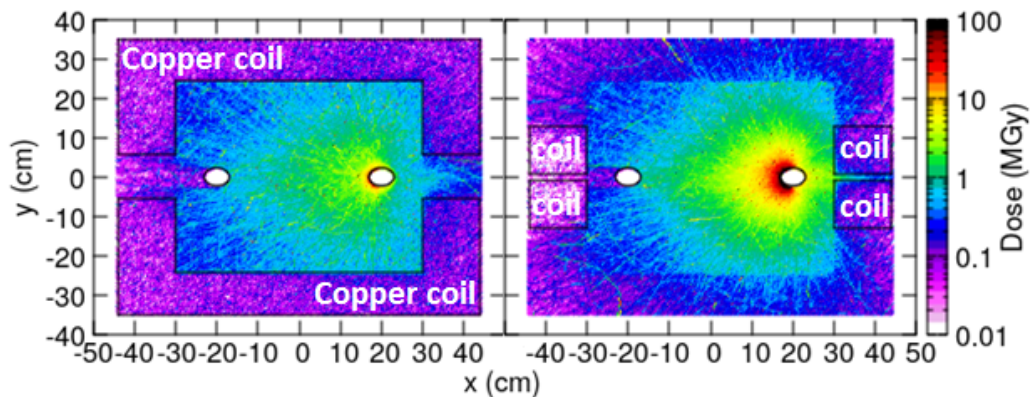
Figure 43: Transverse dose distribution at the MBW.B6 non-IP end, for a cumulative loss amount on the collimation system of 10^{16} top energy protons. Left: Return coil layer. Right: First internal layer. The coil position is indicated. Values are averaged over the respective layer length of 8 cm.

6.1   OZONE PRODUCTION

From the calculation of energy deposition in air, one can estimate the resulting concentration of ozone through the formula:

PRELIMINARY COLLIMATION
SYSTEM DESIGN CONCEPT AND
PERFORMANCE ESTIMATE

EuroCirCol-P3-WP2-
D2.6, EDMS
2041777

Date: 27/02/2019

$$N_{O_s}(ppm) = 9.28 \times 10^{-15} \times G(eV^{-1})\frac{P_{eV}(\frac{eV}{s})\tau(s)}{V(cc)}[1 - e^{\frac{-t}{\tau}}] \qquad (3)$$

where the numerical constant is the ratio between the O_2 concentration and the number of air molecules per cm^3, G is the number of O_3 molecules produced by the absorption of 1 eV (typically 0.06 to 0.074eV^{-1}) and

$$\tau(s) = \frac{1}{(\alpha + \frac{1}{\tau_{vent}} + \frac{kP_{eV}}{V})} \qquad (4)$$

being

$$\alpha(\frac{1}{s}) = 2.3e-4 \qquad \& \qquad k(eV^{-1}cm^3) = 1.4 \times 10^{-16} \qquad (5)$$

the ozone dissociation and decomposition constants, respectively. The second addend of the sum in 4 is the air renewal rate, i.e. the inverse of the ventilation time τ_{vent} needed to fully renew the considered volume of air V.

In our model, the assumption of an average loss rate corresponding to 10^{16} protons per beam lost in the collimation system over an annual operation time of 5000 beam-hours yields a power deposition of 100 W in an air volume of 58000 m^3. Since $\frac{1}{\alpha} = 1.2$ h, a ventilation time larger than several hours would give for this power density in air an ozone concentration of 0.03 ppm. To achieve a factor 10 reduction, a ventilation time of 8 minutes would ideally be required.

7 COLLIMATOR ROBUSTNESS

Preliminary finite element analyses have been conducted on the most loaded TCS and TCP jaws. Simulations were carried out using the finite element software Ansys v18.2. To begin with, a thermal analysis was performed, using as input the beam-induced energy deposition from FLUKA, described in Sec. 6. A static structural analysis was then coupled to the thermal study to obtain the mechanical response of the system. A detailed explanation of the method and of the adopted relevant assumptions can be found in Ref. [56].

Starting from LHC specifications, CFC is adopted as constitutive material for the most loaded collimators. In this study, both losses during both 1 h and 12 minute BLT are considered for the secondary collimator, while only the 12 minute BLT scenario is taken into account for the TCP. This choice is driven by the fact that the 1h BLT scenario for the TCP involves a smaller amount of power than the 1 h BLT case for the TCS (which features the same overall geometry of the TCP), resulting in a less severe case regarding the assessment of the global response of the system (e.g. in terms of thermally-induced deflections of the jaws). Since the goal is to analyse the robustness of the TCP components, which is mainly affected by energy deposition density peaks, only the more severe case of 12 minute BLT is considered for TCPs.

In the 1 h BLT scenario, the beam-induced power deposition is applied in steady state. For the 12 minute BLT scenario, starting from this steady condition, the associated losses are ramped up during 10 ms and then kept for 10 s, to be subsequently ramped down again in 10 ms to the 1 h BLT load (see Fig. 44).
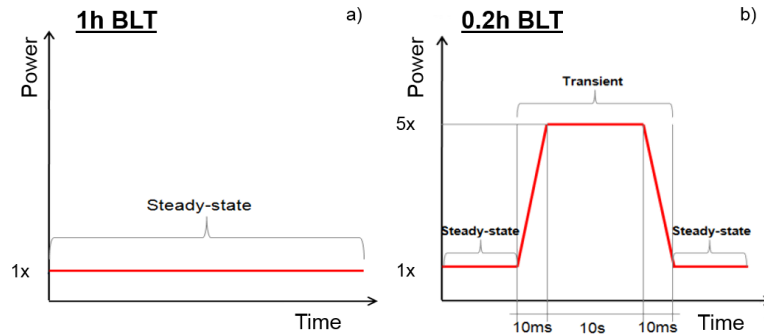
Figure 44: Load profiles considered in the thermo-structural analyses for a) the 1h BLT and b) the 0.2h BLT load case.

All analyses are carried out considering heat loads associated to a design scenario with the skew TCP removed, the TCPs shortened to 30 cm and the thickness of TCPs and TCSs increased to 3.5 cm and to 4.5 cm respectively. Moreover, given the preliminary nature of the study, some simplifying assumptions are made: a perfect bonding between the CFC absorbers and the Glidcop housing is assumed, as well as a linear constitutive law for the absorbers and a constant temperature profile for the water flowing inside the cooling circuit. The following sections discuss the results.

7.1   TCS COLLIMATOR

The design of LHC TCSP collimators is considered as base design for the analysis on the most loaded TCS, namely the TCSG.A6L: the only difference among the two designs is that the former has Glidcop taperings to host the beam position monitors (BPMs), while the latter features CFC taperings (and no BPMs), and that the CFC thickness is increased by 2 cm.
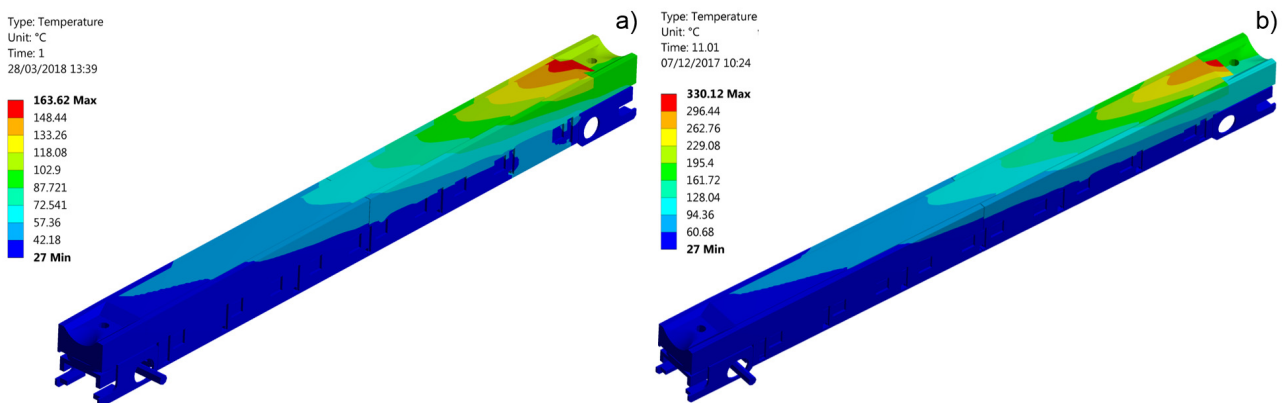

Figure 45: Beam-induced temperature fields on the first TCS for 1 h BLT (left) and 12 minute BLT (right).

The peak temperatures found on the jaw for the 1 h and 12 minute BLT cases are about 164 °C and 330 °C, respectively, as shown in Fig. 45. This induces thermal deformations, strains

**PRELIMINARY COLLIMATION
SYSTEM DESIGN CONCEPT AND
PERFORMANCE ESTIMATE**

**EuroCirCol-P3-WP2-
D2.6, EDMS
2041777**

Date: 27/02/2019

and stresses on the different components, because of the temperature gradient and the thermal-expansion coefficient mismatch among the different materials constituting the jaw. Temporary beam-induced deflections of up to $185\,\mu$m and $246\,\mu$m are obtained for the 1 h and 0.2 h BLT cases, respectively (see Fig. 46). Non-negligible strains are present in the contact region between the CFC absorbers and the housing: these values are mostly due to the bonded contact introduced in the model (perfect bonding) and to the linear character of the constitutive law considered in the analyses for the absorbers, which both lead to an overestimation of the rigidity of the structure.
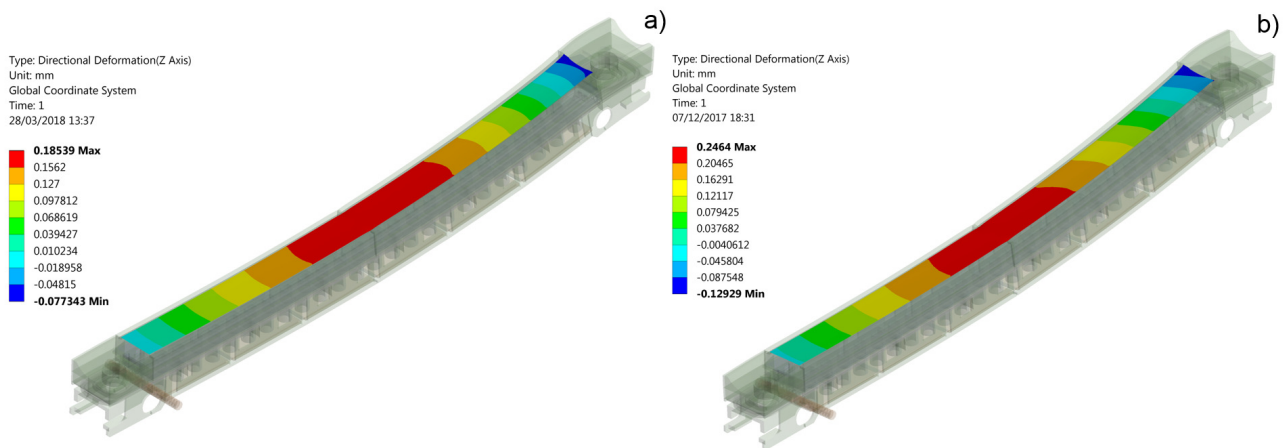
Figure 46: Normal deflections of the TCS jaw for 1 h BLT (left) and 12 minute BLT (right).

Finally, the cooling pipes are found to experience plasticity (see Fig. 47). The elastic limit of the constituting material, CuNi 90-10, is about 100 MPa and it is largely exceeded both in the 1 h and in the 12 minute BLT case. This issue is not a showstopper, as it can be mitigated by adopting a higher yield-strength material for the cooling circuit.

Figure 47: Stress intensity for the first TCS in the CuNi 90/10 cooling pipes for 1 h BLT (left) and 12 minute BLT (right).

7.2 TCP COLLIMATOR

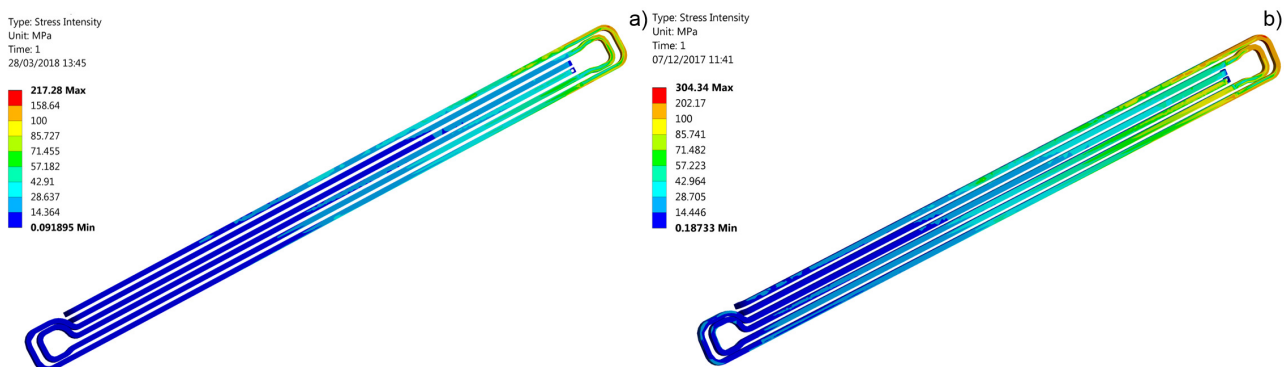As done for TCS collimators, with which they share the same geometry apart form the absorber thickness, the design of LHC TCSP collimators is considered as base design to carry out the analyses also on the vertical TCP, which is exposed to the highest power deposition density peak. In this case, however, only a 30 cm long region of the 3.5 cm thick absorbers has been considered to be subject to power deposition. The maximum temperature found on the CFC is about 660 °C, as shown in Fig. 48: as a result, a maximum stress of 45 MPa is induced in the absorber-housing contact region along the direction normal to the planes constituting the CFC absorber, with an estimated associated strain of about 8000 μm/m, theoretically leading to failure (see Fig. 49).
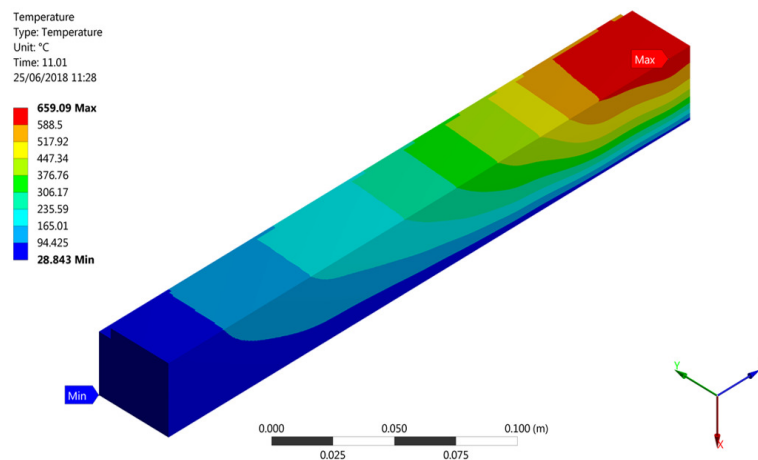
Figure 48: Beam-induced temperature fields on the vertical TCP for the 12 minute BLT case.
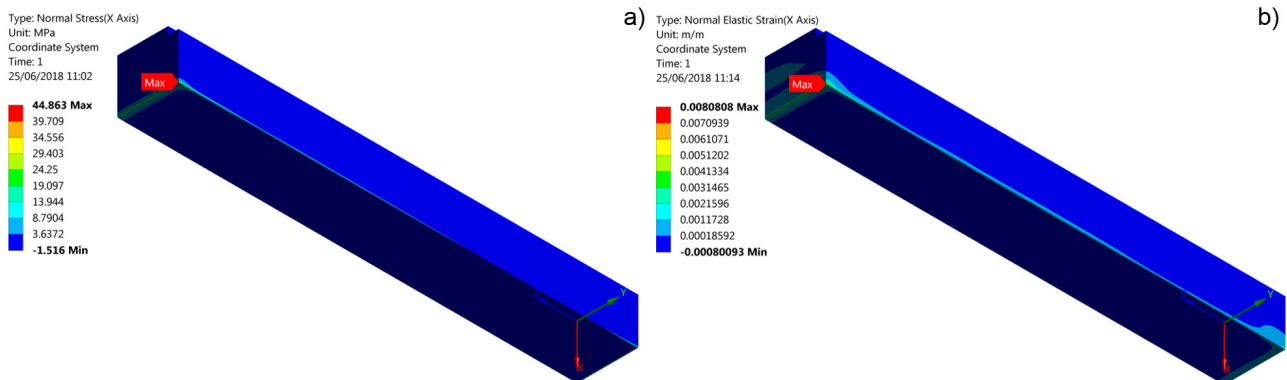
Figure 49: The estimated stress (left) and strain field (right) on the CFC absorber of the vertical TCP for the 12 minute BLT case.

However, similar temperatures have already been achieved repeatdly on CFC absorbers during past experimental campaigns, without reporting any sign of failure [57, 58]. In the HRMT-23 experiment, CFC absorbers reached a peak temperature of 685 °C when impacted by 288-bunches

**PRELIMINARY COLLIMATION
SYSTEM DESIGN CONCEPT AND
PERFORMANCE ESTIMATE**

**EuroCirCol-P3-WP2-
D2.6, EDMS
2041777**

Date: 27/02/2019

with a total intensity of 3.79×10^{13} protons and $\sigma=0.35$mm. Furthermore, in the HRMT-36 experiment, CFC samples experienced a grazing pulse of 288 bunches, with a total intensity of 3.72×10^{13} protons and $\sigma=0.25$ mm. No failure was found in either case, despite thermal gradients which largely exceed those at hand in the present study shown in Fig. 50.
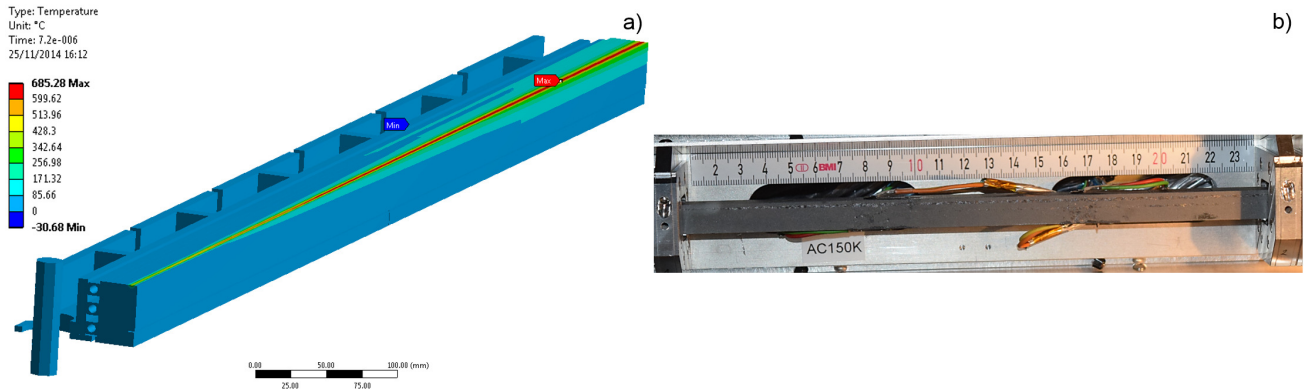
Figure 50: *The temperature field over the CFC absorbers in HRTM-23 [57] (left) and the Mo-coated CFC sample impacted by a grazing shot which melted the coating leaving the CFC substrate unbroken [58] (right).*
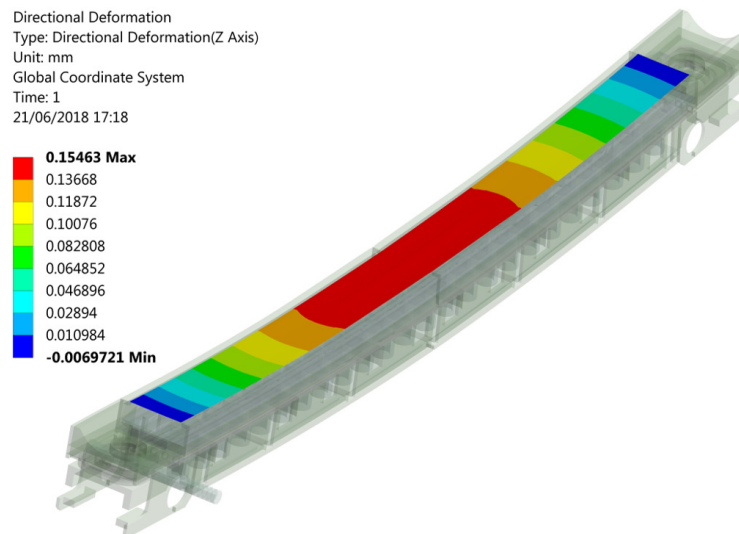

Figure 51: *Beam-induced normal deflection on the vertical TCP for the 12 minute BLT case.*

The obtained high values of stress and strain are therefore thought to be largely due to the simplified nature of the absorber-housing contact adopted in the analysis, as well as to the hypothesis of linear elasticity considered for CFC, Both these assumptions cause a much stiffer structure than the real case. For the same reason, the obtained beam-induced bending deflection of $155\,\mu$m shown in 51 is believed to underestimate the real deformation of the jaw. Regarding the cooling circuit, a maximum stress of 26 MPa is found, much below the elastic limit for CuNi 90-10. No plasticity is observed in the housing either, where a stress peak of 106 MPa is estimated against a yield stress for Glidcop of 294 MPa (see Fig. 52).

PRELIMINARY COLLIMATION
SYSTEM DESIGN CONCEPT AND
PERFORMANCE ESTIMATE

EuroCirCol-P3-WP2-
D2.6, EDMS
2041777

Date: 27/02/2019

Figure 52: Stress intensity in the CuNi 90/10 cooling pipes (left) and the Glicop housing (right) of the vertical TCP during 12 minute BLT losses.

7.3 RESULT ASSESSMENT

Thermo-mechanical analyses conducted on the most loaded TCS and TCP collimators highlighted some critical points which, wi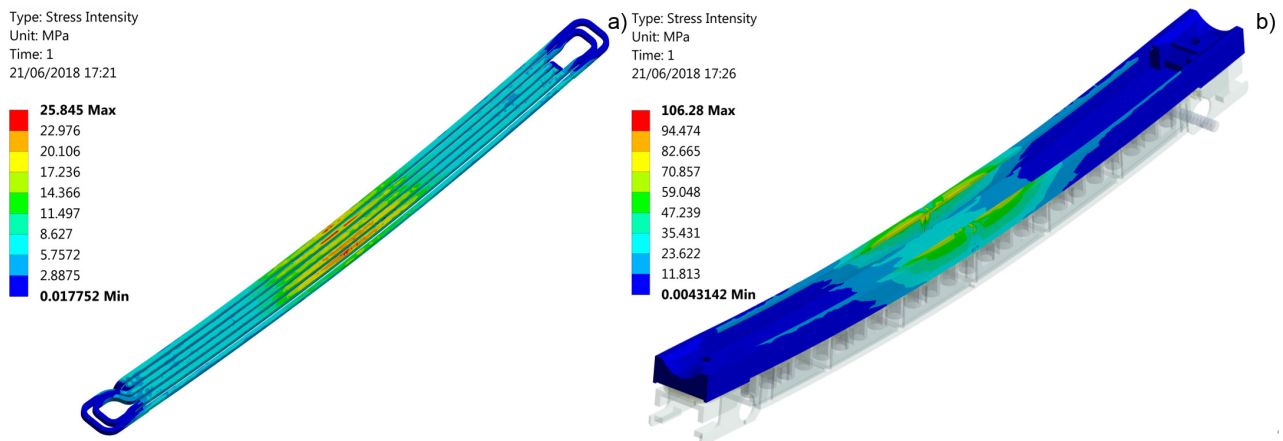thout representing any clear showstopper at this stage, will need to be addressed in future design developments. The only case where permanent deformations occur is in the cooling pipes of the TCS, however, it is believed that this can be mitigated in a straight-forward way by a different material choice for the pipes.

Temperature peaks up to 660 °C are observed in the CFC absorber of the vertical TCP, theoretically leading to failure. However, past tests have shown that no failure occurred in CFC absorbers at these simulated temperatures [57, 58]: the numerical overestimation of stresses and strains is thought to be largely ascribable to the simplifying hypotheses introduced in the numerical models, leading to a stiffer structure. For the same reason an underestimation of the beam-induced bending deflections must be considered for both the case of TCS and TCP, where temporary deformations stay above $100 \mu m$ for all the analysed load cases. It should be assessed in future studies if this has an impact on the cleaning inefficiency. Another potential concern is that the outgassing from graphitic materials such as CFC risks to be very high at the simulated temperatures. The resulting beam vacuum and the possible need for additional pumping should be evaluated in future studies.

Different directions of improvement could be considered to address the points raised above. A summary of proposals would include:

- lighter absorbers, to minimise the energy density on the jaw, e.g. carbon foams [59]

- more rigid housing and stiffener;

- higher water flow in the cooling pipes;

- monitoring, and possibly deformation-correcting, systems. A project in this sense is already launched between CERN and the University of Huddersfield [60]

8 ADVANCED CONCEPTS AND KEY R&D

The studies presented above are based on a collimation system that is scaled up from the LHC but using similar physical hardware. The simulations show that special measures have to be taken to ensure safe operation with acceptable collimator loads during BLT drops, such as the removal of the skew TCP. One important path for general improvements of the collimation system is to study novel materials with improved robustness and acceptable impedance. A more optimized and robust system design could be obtained with such materials if the skew TCP could be kept. A novel mechanical collimator design could also be investigated as an option to further improve the robustness. Furthermore, the cleaning performance might be improved through design iterations on the optics and layout of the two dedicated collimation insertions, and the potential addition of more fixed masks.

Alternative collimation techniques, such as crystal collimation [61] is another path of future study. With this technique, bent crystals are used to channel impacting halo particles and give them an angular kick that is large enough to make them impact deeply at a downstream absorber. Experiments using an LHC test installation [62] have shown a significant improvement of the cleaning efficiency with Pb, Xe, and proton beams [63]. However, since the power deposition of the lost particles will be concentrated on the absorber, its design is very challenging.

Another area of future studies is the control of the beam halo. It has been estimated that for the HL-LHC, the amount of energy present above 3.5 σ is 35 MJ [64]. With a factor 12 higher total stored beam energy in the FCC-hh, the total energy in the halo alone risks to be of the order of 400 MJ, which is more than the total 362 MJ design stored energy of the LHC beam. Any movement or jitter in the orbit risks to cause large losses and beam dumps, that reduce the machine availability. One solution could be to use a hollow electron lens, as studied for HL-LHC [15]. By controlling the diffusion speed of halo particles, one can act on the time profile of the losses, for example by introducing a steady and controlled halo depletion, so that static halo population is significantly reduced. This would reduce the amount of beam scraped during any orbit movement. The parameters and feasibility of a hollow electron lens for FCC-hh remain to be studied.

9 CONCLUSIONS

In this document, a detailed design of the FCC-hh collimation system has been presented, including both the needed collimators and the beam optics. The assumed hardware design of the collimators is based on concepts from the LHC and HL-LHC but with some further developments to cope with the very high power loads expected during the FCC-hh beam loss scenarios. Infrastructure requirements include, as for the LHC, cooling water circuits, controls, and remote inspection and handling and high-radiation areas.

The performance of the FCC-hh collimation system has been studied in detail through particle tracking, energy deposition, and thermo-mechanical simulations. In spite of a stored beam energy of 8.3 GJ, it has been shown that the cleaning performance largely meets the requirements and that the machine can be protected from quenches during lifetime drops down to 12 minutes, which is pessimistically taken as a specification for the betatron cleaning. This has been achieved through the use of a system based on the LHC design but with the addition of extra dispersion suppressor collimators as well as local protection to alleviate losses at some critical locations.

**PRELIMINARY COLLIMATION
SYSTEM DESIGN CONCEPT AND
PERFORMANCE ESTIMATE**

**EuroCirCol-P3-WP2-
D2.6, EDMS
2041777**

Date: 27/02/2019

The cleaning of off-momentum losses at the most critical scenario, where the unbunched beam is lost rapidly at the start of the ramp, has also found to be within the estimated limits.

The collimators themselves will be subject to very high loads during sharp BLT drops and this is a major challenge for the system design. Energy deposition studies and thermo-mechanical simulations have been used to study and optimize the loads, and through changes in the collimator design the resulting peak power load can be brought down to tractable levels. Some issues still remain to be solved but they are not believed to be showstoppers. Other elements in the warm collimation section, such as the passive absorbers and the warm dipoles, receive very high instantaneous power loads, and the design and cooling of these elements need further study and optimization.

PRELIMINARY COLLIMATION
SYSTEM DESIGN CONCEPT AND
PERFORMANCE ESTIMATE

EuroCirCol-P3-WP2-
D2.6, EDMS
2041777

Date: 27/02/2019

10   REFERENCES

[1] M. Fiascaris, *et al.*, "First Design of a Proton Collimation System for 50 TeV FCC-hh," *Proceedings of the International Particle Accelerator Conference 2016, Busan, Korea*, p. 2425, 2016.

[2] M. Fiascaris, R. Bruce, and S. Redaelli, "A conceptual solution for a beam halo collimation system for the Future Circular hadron-hadron Collider (FCC-hh)," *Nuclear Instruments and Methods in Physics Research Section A: Accelerators, Spectrometers, Detectors and Associated Equipment*, vol. 894, pp. 96 – 106, 2018.

[3] J. Molson, *et al.*, "Status of the FCC-hh collimation system," *Proceedings of the International Particle Accelerator Conference 2017, Copenhagen, Denmark*, p. 64, 2017.

[4] M. I. Besana *et al.*, "Energy deposition in the betatron collimation insertion of the 100 TeV future circular collider," *Proceedings of the International Particle Accelerator Conference 2017, Copenhagen, Denmark*, p. 68, 2017.

[5] R. W. Assmann, "Preliminary Beam-based specifications for the LHC collimators," Tech. Rep. LHC-PROJECT-NOTE-277, CERN, Geneva, Jan 2002.

[6] J. B. Jeanneret, "Momentum losses in LHC : the special case of RF uncaptured protons," *CERN SL-Note-92-56-EA*, 1992.

[7] S. Wretborn, *et al.*, "Study of off-momentum losses at the start of the ramp in the Large Hadron Collider," *CERN-ACC-NOTE-2017-0065*, Sep 2017.

[8] R.W. Assmann, "Collimators and Beam Absorbers for Cleaning and Machine Protection," *Proceedings of the LHC Project Workshop - Chamonix XIV, Chamonix, France*, p. 261, 2005.

[9] G. Robert-Demolaize, *Design and Performance Optimization of the LHC Collimation System*. PhD thesis, Universite Joseph Fourier, Grenoble, 2006.

[10] R.W. Assmann *et al.*, "The Final Collimation System for the LHC," *Proc. of the European Particle Accelerator Conference 2006, Edinburgh, Scotland*, p. 986, 2006.

[11] C. Bracco, *Commissioning Scenarios and Tests for the LHC Collimation System*. PhD thesis, EPFL Lausanne, 2008.

[12] R. Bruce *et al.*, "Simulations and measurements of beam loss patterns at the CERN Large Hadron Collider," *Phys. Rev. ST Accel. Beams*, vol. 17, p. 081004, Aug 2014.

[13] R. Bruce, R. W. Assmann, and S. Redaelli, "Calculations of safe collimator settings and β^* at the CERN Large Hadron Collider," *Phys. Rev. ST Accel. Beams*, vol. 18, p. 061001, Jun 2015.

[14] R. Bruce, *et al.*, "Reaching record-low β^* at the CERN Large Hadron Collider using a novel scheme of collimator settings and optics," *Nucl. Instr. Meth. Phys. Res. A*, vol. 848, pp. 19 – 30, Jan 2017.

[15] G. Apollinari, *et al.*, *High-Luminosity Large Hadron Collider (HL-LHC): Technical Design Report V. 0.1*. CERN Yellow Reports: Monographs. CERN-2017-007-M, Geneva: CERN, 2017. R. Bruce, https://cds.cern.ch/record/2284929.

[16] R. Bruce, A. Marsili, and S. Redaelli, "Cleaning Performance with 11T Dipoles and Local Dispersion Suppressor Collimation at the LHC," *Proceedings of the International Particle Accelerator Conference 2014, Dresden, Germany*, p. 170, 2014.

[17] A. Lechner, *et al.*, "Power Deposition in LHC Magnets With and Without Dispersion Suppressor Collimators Downstream of the Betatron Cleaning Insertion," *Proceedings of the International Particle Accelerator Conference 2014, Dresden, Germany*, p. 112, 2014.

[18] A. Marsili, R. Bruce, and S. Redaelli, "Collimation Cleaning for HL-LHC Optics Scenarios with Error Models," *Proceedings of the International Particle Accelerator Conference 2014, Dresden, Germany*, p. 163, 2014.

[19] G. Valentino, *et al.*, "Successive approximation algorithm for beam-position-monitor-based LHC collimator alignment," *Phys. Rev. ST Accel. Beams*, vol. 17, p. 021005, 2014.

[20] R. Bruce, *et al.*, "Parameters for HL-LHC aperture calculations and comparison with aperture measurements," *CERN Report CERN-ACC-2014-0044*, 2014.

[21] R. Bruce, *et al.*, "Parameters for aperture calculations at injection for HL-LHC," *CERN-ACC-2016-0328*, 2016.

[22] R. Bruce, *et al.*, "Updated parameters for HL-LHC aperture calculations for proton beams," *CERN-ACC-2017-0051*, 2017.

[23] "MAD-X program." http://cern.ch/mad/.

[24] C. A. Pons, *et al.*, "LHC aperture measurements," *Proceedings of IPAC 10, Kyoto, Japan*, p. 477, 2010.

[25] C. A. Pons, *et al.*, "IR1 and IR5 aperture at 3.5 TeV," *CERN-ATS-Note-2011-110 MD*, 2011.

[26] R. Assmann, *et al.*, "Aperture Determination in the LHC Based on an Emittance Blowup Technique with Collimator Position Scan," *Proceedings of IPAC11, San Sebastian, Spain*, p. 1810, 2011.

[27] S. Redaelli, *et al.*, "Aperture measurements in the LHC interaction regions," *Proceedings of IPAC12, New Orleans, Louisiana, USA*, p. 508, 2012.

[28] C. A. Pons, *et al.*, "IR2 aperture measurements at 3.5 TeV," *CERN-ATS-Note-2012-017 MD*, 2012.

[29] R. Bruce, *et al.*, "IR8 aperture measurements at injection energy," *CERN-ATS-Note-2013-026 MD*, 2013.

**PRELIMINARY COLLIMATION
SYSTEM DESIGN CONCEPT AND
PERFORMANCE ESTIMATE**

**EuroCirCol-P3-WP2-
D2.6, EDMS
2041777**

Date: 27/02/2019

[30] R. Bruce, *et al.*, "IR2 aperture measurements at 4.0 TeV," *CERN-ACC-NOTE-2013-0011 MD*, 2013.

[31] P. Hermes, *et al.*, "Improved Aperture Measurements at the LHC and Results from their Application in 2015," *Proceedings of the International Particle Accelerator Conference 2016, Busan, Korea*, p. 1446, 2016.

[32] N. Fuster-Martinez, R. Bruce, and S. Redaelli, "LHC β^*-reach MD: aperture measurements at small β^*," *CERN-ACC-NOTE-2017-0064*, Nov 2017.

[33] N. Fuster-Martinez and E. Maclean and J. Dilly and R. Bruce and R. Tomas and S. Redaelli and T. Persson and L. Nevay, "Aperture measurements with AC dipole," *CERN-ACC-NOTE-2018-0008*, Feb 2018.

[34] M. Benedikt *et al.*, "Future Circular Collider Study. Volume 3: The Hadron Collider (FCC-hh) Conceptual Design Report," Tech. Rep. CERN-ACC-2018-0058, CERN, Geneva, Dec 2018. Submitted for publication to Eur. Phys. J. ST.

[35] J.B. Jeanneret, "Geometrical tolerances for the qualification of LHC magnets," *LHC Project Report 1007, CERN*, 2006.

[36] A. Mereghetti *et al.*, "Sixtrack-FLUKA active coupling for the upgrade of the SPS scrapers," *Proceedings of the International Particle Accelerator Conference 2013, Shanghai, China*, p. 2657, 2013.

[37] A. Mereghetti, *Performance Evaluation of the SPS Scraping System in View of the High Luminosity LHC*. PhD thesis, University of Manchester, 2015.

[38] E. Skordis, *et al.*, "FLUKA coupling to Sixtrack," *CERN-2018-011-CP, Proceedings of the ICFA Mini-Workshop on Tracking for Collimation, CERN, Geneva, Switzerland*, p. 17, 2018.

[39] F. Schmidt, "SixTrack. User's Reference Manual," *CERN/SL/94-56-AP*, 1994.

[40] G. Robert-Demolaize, *et al.*, "A new version of SixTrack with collimation and aperture interface," *Proc. of the Particle Accelerator Conf. 2005, Knoxville*, p. 4084, 2005.

[41] "Sixtrack web site." http://sixtrack.web.cern.ch/SixTrack/.

[42] A. Ferrari, *et al.*, "FLUKA: a multi-particle transport code," *CERN Report CERN-2005-10*, 2005.

[43] T. Bohlen, *et al.*, "The FLUKA Code: Developments and Challenges for High Energy and Medical Applications," *Nuclear Data Sheets*, no. 120, pp. 211–214, 2014.

[44] B. Auchmann *et al.*, "Testing beam-induced quench levels of LHC superconducting magnets," *Phys. Rev. ST Accel. Beams*, vol. 18, p. 061002, 2015.

[45] J. B. Jeanneret *et al*, "Quench levels and transient beam losses in LHC magnets," *LHC Project Report 44, CERN*, 1996.

PRELIMINARY COLLIMATION
SYSTEM DESIGN CONCEPT AND
PERFORMANCE ESTIMATE

EuroCirCol-P3-WP2-
D2.6, EDMS
2041777

Date: 27/02/2019

[46] L. Bottura *et al.*, "Expected performance of 11T and MB dipoles considering the cooling performance," *Presentation at 8th HL-LHC collaboration meeting, CERN, Geneva Switzerland*, 2018.

[47] M. Varasteh *et al.*, "Cold loss studies for the quench limit assessment," in *4th EuroCirCol Meeting*, Oct 2018.

[48] C. Collaboration, "Absolute Calibration of Luminosity Measurement at CMS: Summer 2011 Update," Tech. Rep. CMS-PAS-EWK-11-001, CERN, Geneva, 2011.

[49] R. Tomas, private communication.

[50] G. Battistoni *et al.*, "Overview of the FLUKA code," *Annals Nucl. Energy*, vol. 82, pp. 10–18, 2015.

[51] A. Krainer, "Design and Simulation of new protection devices in the dispersion suppressor regions for the Future Circular Collider Project (to be published)," Master's thesis, Graz University of Technology, Austria, 2019.

[52] J. Molson, *et al.*, "Simulating the LHC collimation system with the accelerator physics library MERLIN," *Proceedings of ICAP12, Rostock-Warnemünde, Germany*, pp. 12–14, 2012.

[53] M. Serluca *et al.*, "HI-LUMI LHC collimation studies with MERLIN code," *Proceedings of the International Particle Accelerator Conference 2014, Dresden, Germany*, p. 784, 2014.

[54] A. Chancé *et al.*, "Updates on the Optics of the Future Hadron-Hadron Collider FCC-hh," *Proceedings of the International Particle Accelerator Conference 2017, Copenhagen, Denmark*, p. 2023, 2017. TUPVA002.

[55] D. Tommasini *et al.*, "Status of the 16 T Dipole Development Program for a Future Hadron Collider," *IEEE Trans. Appl. Supercond.*, vol. 28, no. 3, p. 4001305. 5 p, 2018.

[56] A. Dallocchio, *Study of thermomechanical effects induced in solids by high-energy particle beams: analytical and numerical methods.* PhD thesis, CERN-THESIS, 2008.

[57] F. Carra, *et al.*, "New TCSPM Design Outcome of HRMT-23: Robustness of HL-LHC jaws." Special LHC Collimation Upgrade Specification Meeting: Material and design readiness for LS2 productions, CERN, 2017.

[58] A. Bertarelli, *et al.*, "HRMT-36 (Multimat) Experiment: Preliminary Results." LHC Collimation Upgrade Specification Meeting N° 96, CERN, 2017.

[59] E. Quaranta, *et al.*, "Towards optimum material choices for the HL-LHC collimator upgrade." IPAC16, Busan, Korea, 2016.

[60] T. Furness, "Design and integration of an active dynamic compensation for the collimator jaw in the Multimat experiment." Eucard2 WP11 topical meeting, CERN, 2017.

[61] D. Mirarchi, *Crystal Collimation for LHC.* PhD thesis, Imperial College London, 2015.

[62] D. Mirarchi, *et al.*, "Design and implementation of a crystal collimation test stand at the Large Hadron Collider," *The European Physical Journal C*, vol. 77, p. 424, Jun 2017.

[63] W. Scandale *et al.*, "Observation of channeling for 6500 GeV/c protons in the crystal assisted collimation setup for LHC," *Physics Letters B*, vol. 758, pp. 129 – 133, 2016.

[64] R. Appleby *et al.*, "Report from the Review Panel," *Review of the needs for a hollow electron lens for the HL-LHC, CERN, Geneva, Switzerland*, 2016.